CHALMERS
UNIVERSITY OF TECHNOLOGY

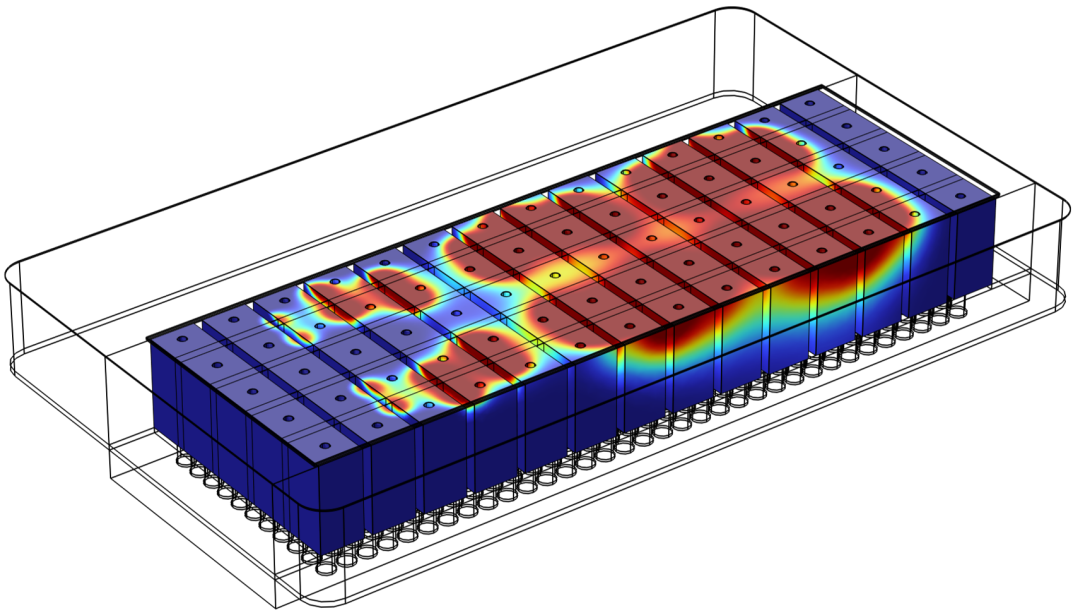

Enhancing thermal management in battery electric vehicles using phase change materials

Master's thesis in Sustainable Electric Power Engineering and Electromobility

Yang Zhang

DEPARTMENT OF MECHANICS AND MARITIME SCIENCES

CHALMERS UNIVERSITY OF TECHNOLOGY
Gothenburg, Sweden 2025
www.chalmers.se

Master's thesis 2025

Enhancing Thermal Management in Battery Electric Vehicles Using Phase Change Materials

Yang Zhang

CHALMERS
UNIVERSITY OF TECHNOLOGY

Department of Mechanics and Maritime Sciences
Division of Vehicle Engineering and Autonomous Systems.
Chalmers University of Technology
Gothenburg, Sweden 2025

Enhancing Thermal Management in Battery Electric Vehicles Using Phase Change Materials

YANG ZHANG

Supervisor: Hamed Jamshidi, Volvo Cars
Examiner: Simone Sebben, Chalmers Department of Mechanics and Maritime Sciences

Master's Thesis 2025
Department of Mechanics and Maritime Sciences
Division of Vehicle Engineering and Autonomous Systems
Chalmers University of Technology
SE-412 96 Gothenburg
Telephone +46 79 352 8428

Cover: Solid-liquid distribution during the phase change of PCM as shown in Comsol.

Typeset in LaTeX
Printed by Chalmers Reproservice
Gothenburg, Sweden 2025

Enhancing Thermal Management in Battery Electric Vehicles Using Phase Change Materials
YANG ZHANG
Department of Mechanical and Maritime Sciences
Chalmers University of Technology

Abstract

With the development of the e-mobility industry, the thermal management of power electronic devices such as inverters in battery electric vehicles (BEVs) has become increasingly prominent, especially with today's trend of high power density and system integration, where traditional cooling methods face many challenges. This thesis focuses on the application of phase change materials (PCMs) in the thermal management of inverters, aiming to improve the thermal management system temperature control capability. First, an inverter power loss model considering switching loss and conduction loss is constructed in matlab to simulate the inverter power loss under real driving conditions. On this basis, a fluid-thermal coupling simulation model was constructed in COMSOL Multiphysics to analyze the thermal response of PCM materials under different layout configurations. This study systematically evaluates the effects of various PCM layouts on temperature rise control and optimizes their thermal buffer performance while satisfying the volume constraints. The simulation results show that a reasonably designed PCM thermal management scheme can significantly reduce the peak temperature of key inverter components and lower the rate of temperature change to reduce the thermal shock, thus improving the thermal stability and reliability of the system and extending the service life of the inverter. This study provides a theoretical basis and engineering reference for the design of an efficient and compact thermal management system for electric vehicles.

Keywords: Battery Electric Vehicle (BEV); Inverter; Thermal Management; Phase Change Material (PCM); Multiphysics Simulation; Power Loss Modeling; COMSOL; Thermal Reliability.

Acknowledgements

This thesis demonstrates my long and in-depth exploration of high-fidelity multi-physics field simulation and optimization.
I would like to express my sincere gratitude to Volvo Cars for providing me with this program, which has provided me with invaluable hands-on opportunities.
First and foremost, I would like to express my sincere gratitude to my supervisor, Dr. Hamed Jamishidi, whose clear guidance, technical expertise, and continuous encouragement played a crucial role throughout the research process, and who was always available to provide timely and valuable comments to show the way forward.
I would also like to thank my examiner, Prof. Simone Sebben, for her invaluable feedback which helped me to refine my research.
In addition to this a special thanks to my colleagues and friends in the company who helped make the research process fun. I would also like to give a special thanks to my teammate Henry, whose cooperation, creativity and teamwork helped me understand how I can work better as a team to solve problems.
Finally, I would like to thank all the people who supported me. This project has not only enriched my knowledge, but also given me a meaningful personal experience!

Yang Zhang, Gothenburg, 2025

List of Acronyms

Below is the list of acronyms that have been used throughout this thesis:

EVs	Electrical Vehicles
BEVs	Battery Electrical Vehicles
AC	Alternating Current
DC	Direct Current
PCM	Phase Change Materials
NePCM	PCM with nanocomposite added
TCE	Thermal Conductivity Enhancer
PCM-HEX	PCM Heat Exchanger
HTF	Heat transfer fluid
MF	Metal Foam
PPI	Pores Per Inch
MOSFET	Metal–Oxide–Semiconductor Field-Effect Transistor
FOC	Field-oriented control
BOBYQA	Bound Optimization BY Quadratic Approximation

Symbols

ρ	Air Density[kg/m^3]
C_d	Air resistance coefficient
A	Windward area[m^2]
v	Velocity[m/s]
F_{drag}	Air resistance[N]
a	Acceleration[m/s^2]
$F_{rolling}$	Rolling resistance[N]
μ	Rolling resistance coefficient
m	Mass of the car[Kg]
ω_{motor}	Motor speed
r_w	Wheel radius[m]
G	Gear ratio
T_{wheel}	Wheel output torque[N/m]
T_{motor}	Motor output torque[N/m]
I_d	d-axis curren[A]
ω_{base}	Base speed
λ_m	Permanent magnetic flux[Wb]
L_d	d-axis inductance[H]
I_q	q-axis curren[A]
L_q	q-axis inductance[H]
I_{stator}	Stator current [A]
ϕ	Porosity
V_{void}	Volume of pores in metal foam
V_{solid}	Solid volume in metal foam
V_{total}	Total volume of metal foam
t	Time instant [s]

$i_a(t), i_b(t), i_c(t)$	Phase currents of PMSM in phases a, b, c [A]
$u_{x+}(t), u_{x-}(t)$	Switching states of the upper (+) and lower (-) switches in phase x ($x = a, b, c$), dimensionless (1 = ON, 0 = OFF)
$i_{S_{x+}}(t), i_{S_{x-}}(t)$	Instantaneous current through the upper (+) and lower (-) switching device of phase x [A]
$\omega = 2\pi f_m$	Angular frequency of the fundamental modulation component
f_{sw}	Switching frequency of the PWM carrier
$v_{mx}(t)$	Modulation voltage signals for phases x
S_1 to S_6	Six inverter MOSFET switches
2 μs	Dead-time inserted between upper and lower switches
$I_{\text{sw}}(t)$	Instantaneous current through each switching device
$\lvert I_{\text{sw}}(t) \rvert$	Absolute value of instantaneous current (used for energy lookup)
$V_{\text{on}}(I_{\text{sw}}, T_j)$	On-state voltage drop as a function of current and junction temperature
$E_{\text{on}}(I_{\text{sw}}, T_j)$	Turn-on switching energy loss from datasheet lookup
$E_{\text{off}}(I_{\text{sw}}, T_j)$	Turn-off switching energy loss from datasheet lookup
$P_{\text{cond}}(t)$	Instantaneous conduction loss power
$P_{\text{sw}}(t)$	Instantaneous switching loss power
$P_{\text{total}}(t)$	Total instantaneous inverter power loss
$V_{\text{dc}}(t)$	Instantaneous DC bus voltage
V_{ref}	Reference DC voltage for datasheet losses
T_j	Junction temperature (assumed constant at 25°C)

Contents

List of Figures

List of Tables

1

Introduction

1.1 Background

With the continuous growth of the global motor vehicle population, greenhouse gas emissions have shown a significant upward trend, which is particularly prominent in developing countries. Driven by the dual drive of economic development stage and urbanization process, this emission trend will continue to grow inertia in the foreseeable medium and long term (Jaramillo et al., 2022). To meet this environmental challenge, electric transportation (E-mobility) has emerged as a sustainable solution, the core of which is the adoption of a new generation of clean energy vehicles. Among many technical paths, electric vehicles (EVs) have been widely regarded as the most promising low-carbon transportation option due to their significant potential for carbon emission reduction and advantages of technological advancement (Cambridge University Press, n.d.).

However, the development of electric vehicles has always faced challenges due to energy conversion issues. One way to solve this problem is to use high-efficiency and high-power density electronic devices (Jaguemont, Boulon and Dubé, 2016; Zhang et al., 2020). The motor inverter is one of the important electronic modules in the power part of electric vehicles and plays a vital role in the overall energy efficiency of the vehicle. It converts the DC power in the battery into the AC power required by the motor. The inverter contains transistor modules, which are subjected to very high heat flux. The heat load generated by the transistor module at full load is 100-150 W/cm2, which is expected to increase to 500 $W/cm2$ in the future due to the increase in current capacity and switching frequency (Wang et al., 2022). The temperature of the inverter will also affect its output power, which in turn affects the normal operation of electric vehicles, so we need to develop advanced thermal management technologies that can handle high heat flux density (Cai et al., 2016; Erp, Georgios Kampitsis and Elison Matioli, 2019). Using a proper cooling system can effectively improve the performance of the inverter (Lajunen, Yang and Emadi, 2018).

To stabilize the inverter temperature, researchers have developed a variety of efficient cooling technologies for tram inverters (Chang et al., 2017; Gautier Rouaze et al., 2021; Lei, Xin and Liu, 2022; Wang et al., 2022b). Han et al. conducted an experimental study on the heat dissipation performance of various heat sinks and found the heat sink with the best overall performance - serpentine heat sink, which has good heat transfer ability. In addition, they also optimized the overall structure of

the heat sink (Han, Guo and Ding, 2021). Bostanci et al. conducted an experimental study on the performance of spray cooling in motor inverter cooling. When using spray cooling, the maximum heat flux that the inverter can withstand is $400/cm^2$ and the temperature can be kept below $150°C$(Huseyin Bostanci et al., 2012). Wang et al. (2023) systematically studied the thermodynamic performance of the Toyota Prius inverter under single-phase and two-phase cooling conditions by combining theoretical analysis and numerical simulation methods. The research team used R134a refrigerant as the two-phase cooling medium and water as a single-phase cooling control. The experimental data showed that compared with the traditional single-phase cooling system, the two-phase cooling technology showed significant advantages in key performance indicators (Wang, McCluskey and Bar-Cohen, 2013).

In addition to the significant thermal load of the inverter under steady-state operating conditions, the transient characteristics of the electric vehicle power system also pose a key challenge. Specifically, when the vehicle is accelerating suddenly, the inverter output power increases in a step-like manner, and its response time constant is very low. This dynamic response mismatch causes the thermal sensor and the cooling system to be unable to track temperature changes in a timely manner, which in turn leads to a serious consequence: Thermal cycle stress increases, reducing the life of the inverter. Using PCM technology is one way to solve this problem.

Phase Change Materials (PCMs) are a type of thermal management medium that undergoes a phase change within a characteristic phase change temperature zone. Their thermodynamic properties are manifested in temperature control through the isothermal absorption/release of latent heat during the phase change process. Based on their high heat capacity characteristics and dynamic thermal response capabilities, this type of material can effectively buffer transient thermal shocks, and is therefore particularly suitable for inverter thermal management systems with intermittent power characteristics, showing significant advantages in improving energy conversion efficiency and equipment operation sustainability. The key parameter for material selection is the characteristic phase change temperature. To achieve optimal thermal management performance, it is necessary to ensure that the melting point of the PCM is close to the actual operating temperature of the inverter(İsmail Gürkan Demirkıran, Oliveira and Erdal Cetkin, 2022; Mehwish Mahek Khan et al., 2023). Although it is undeniable that although PCM has excellent thermal management performance, it also faces some problems, such as low thermal conductivity and stability in multiple cycles (Gil et al., 2010).To address these issues, many researchers have tried different approaches such as using thermal conductivity enhancers (fins, metal foams, nanoparticles), using different geometries of heat transfer surfaces, packaging techniques, and hybrid PCM material development (Al-Salami et al., 2024; Low, Qin and Duan, 2024).Among these methods, the use of metal foam can significantly improve the performance of PCM, and metal foams with different porosity and PPI have different abilities to improve PCM performance. PPI (Pores Per Inch) refers to the number of pores within one linear inch of the material (Cui et al., 2022; Shi et al., 2023).

In this thesis, a new heat sink design for vehicle inverter using PCM and metal foam is proposed with the objective, and its heat dissipation capacity under actual driving cycle is simulated. At the same time, there is no research on the thermal resistance of metal foams with different porosities when used together with PCM in the current literature.

1.2 Objectives

The aim of this master's thesis is to design a new vehicle inverter cooling device that utilizes PCM as a cooling enhancer to improve the thermal management performance of the inverter and enhance its ability to cope with power surges. In the initial phase of the project, MATLAB is utilized to develop a comprehensive power loss model for the inverter. The power loss of the inverter is accurately evaluated using actual driving condition data as inputs and is used as the main heat source for thermal management simulation. After that, COMSOL Multiphysics was utilized for detailed design and analysis to simulate the thermal performance of the heat sink under different design parameters. Through iterative optimization, the configuration with the best thermal management performance is determined.

2

Theory

This chapter highlights the most important basic points of the paper and introduces the theoretical ideas of electrical engineering, heat transfer and materials science behind the design and numerical simulation.

2.1 Inverter loss model construction

Power electronics play a key role in converting the electrical energy in the battery to a traction motor. Figure 2.1 illustrates one possible configuration of an electric vehicle powertrain. An inverter converts the DC current flowing from the battery system into the required AC current, which is then fed into the electric motor to provide kinetic energy for the electric vehicle.

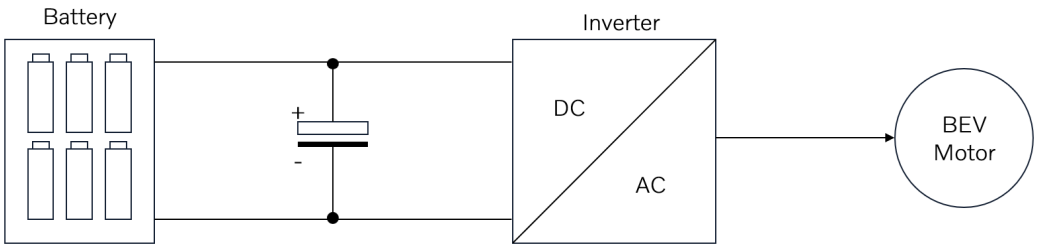

Figure 2.1: Electric vehicle powertrain configuration

During the operation of an electric vehicle, the power semiconductor devices in the inverter generate conduction and switching losses. The heat generated by these losses leads to an increase in chip temperature, which in turn affects performance and reliability. This study focuses on the thermal behavior of the inverter under frequent and rapid acceleration and deceleration conditions. Based on a specific driving condition, the power loss of the inverter is calculated and thermally analyzed in COMSOL as a heat source to evaluate the temperature distribution and heat dissipation characteristics. The driving conditions used are shown in Figure 2.2.

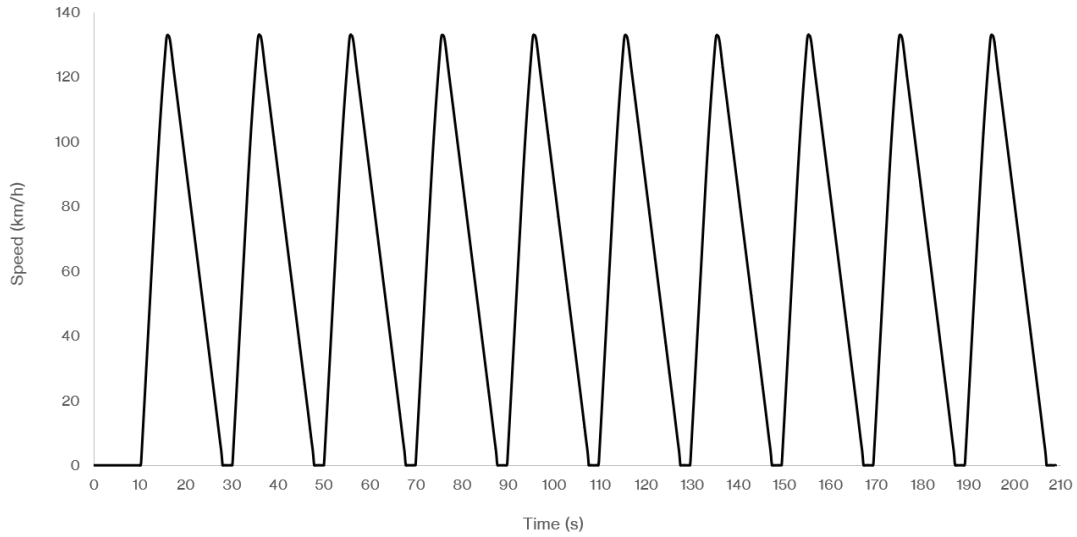

Figure 2.2: Drive Cycle

The following detailed calculation of the inverter losses of the electric vehicle for this driving condition is carried out. The required traction force is calculated by vehicle dynamics analysis to further derive the motor speed and torque. Subsequently, based on the vector control strategy, the d-axis and q-axis current calculations under weak magnetic control are considered to finally obtain the motor stator current and inverter input current. Then, the losses are calculated by combining the inverter input current and the inverter operating principle.

2.1.1 Vehicle dynamics calculations

A vehicle needs to overcome a variety of external resistances during driving, including rolling resistance when the car is driving on a flat road, air resistance, and inertia during acceleration.In this

$$F_{drag} = \frac{1}{2}\rho C_d A v^2 \tag{2.1}$$

where F_{drag} is air resistance, which comes from the force of air on the vehicle, and its magnitude is proportional to the square of the vehicle's speed. ρ is the air density, C_d is air resistance coefficient, A is the vehicle's frontal area, v is the velocity. The vehicle's acceleration is calculated from the velocity data using the numerical differentiation method:

$$a = \frac{dv}{dt} \tag{2.2}$$

For rolling resistance $F_{rolling}$

$$F_{rolling} = \mu m g \tag{2.3}$$

where μ is rolling resistance coefficient, m is the mass of the car, g is the gravity acceleration.When the car is driving on a flat road, the total vehicle traction is

$$F_{traction} = m \cdot a + F_{drag} + F_{rolling} \tag{2.4}$$

2.1.2 Motor speed and output torque calculations

The motor speed depends on the wheel speed and the transmission ratio, and is calculated as follows

$$\omega_{motor} = \frac{v}{r_w} \cdot G \tag{2.5}$$

where r_w is wheel radius, G is gear ratio, the wheel output torque is determined by the traction and wheel radius, as shown in the formula

$$T_{wheel} = F_{traction} \cdot r_w$$

Furthermore, the motor output torque is determined by the wheel torque and the transmission ratio:

$$T_{motor} = \frac{T_{wheel}}{G} = \frac{F_{traction} \cdot r_w}{G} \tag{2.6}$$

2.1.3 Motor current calculation

2.1.3.1 Field weakening control strategy

In a Field Oriented Control (FOC) strategy, the d-axis current (I_d) is primarily used to regulate the magnetic field. When the motor is running below the base speed, I_d is typically set to 0 to maintain the maximum torque-to-current ratio. However, when the motor speed exceeds the base speed (ω_{base}), magnetic field weakening control is required to maintain constant power operation by applying a negative I_d to reduce the magnetic flux:

$$I_d = \begin{cases} 0 & \omega_{motor} \leq \omega_{base} \\ -\frac{(\omega_{motor} - \omega_{base}) \cdot \lambda_m}{L_d} & \omega_{motor} > \omega_{base} \end{cases} \tag{2.7}$$

where λ_m is permanent magnetic flux,L_d is d-axis inductance

2.1.3.2 q-axis current

The q-axis current (I_q) is mainly used to generate electromagnetic torque, and its calculation formula is as follows:

$$I_q = \frac{T_{motor}}{1.5p(\lambda_m + (L_q - L_d)I_d)} \tag{2.8}$$

where p is motor pole pairs, L_q is q-axis inductance,the formula shows that when weak magnetic control is used, the d-axis current will affect the calculation of the q-axis current.

2.1.3.3 Stator current

The three-phase stator current of the motor is calculated from I_d and I_q

$$I_{stator} = \sqrt{I_d^2 + I_q^2} \tag{2.9}$$

this current is used to evaluate the motor operating status and its current demand on the inverter

2.1.4 Inverter input current calculation

After getting the phase current waveforms of the PMSM in one drive cycle, the next step is to estimate the current waveforms of each switching device in the inverter. This is critical for subsequent loss calculations.Consider a three-phase two-level inverter with six switching devices (one up and one down switch per phase). This is critical for subsequent loss calculations.

2.1.4.1 Inverter Topology and Switching Signals

The inverter we study is controlled using the third harmonic injection space vector PWM (SVPWM) method while having a fixed switching frequency f_s according to the relevant tables, and we also need to insert a dead time t_{dead}.
The switching signal of each upper switch S_{x+} $(x = a, b, c)$ is generated according to the PWM modulation index and switching frequency, and the dead time is added to avoid breakdown.

2.1.4.2 Deriving Device Currents from Phase Currents and Switching States

At any given moment t, the instantaneous current flowing through each switching device depends on the corresponding phase current and switching state.
For a-phase, $i_a(t)$ means instantaneous phase current, and $u_{a+}(t)$ and $u_{a-}(t)$ means the switching state of the upper and lower switches, respectively (+ means on, - means off). Then the currents flowing through the upper and lower switching devices in phase a are given by the following equation:

$$i_{S_{a+}}(t) = u_{a+}(t) \cdot i_a(t) \tag{2.10}$$

$$i_{S_{a-}}(t) = u_{a-}(t) \cdot (-i_a(t)) \tag{2.11}$$

Where the negative sign indicates that the direction of the current in the lower switch is opposite to the phase current, which represents the renewal or reverse conduction current.
Similarly, for phases b and c:

$$i_{S_{b+}}(t) = u_{b+}(t) \cdot i_b(t), \quad i_{S_{b-}}(t) = u_{b-}(t) \cdot (-i_b(t)) \tag{2.12}$$

$$i_{S_{c+}}(t) = u_{c+}(t) \cdot i_c(t), \quad i_{S_{c-}}(t) = u_{c-}(t) \cdot (-i_c(t)) \tag{2.13}$$

The instantaneous input DC current $i_{dc}(t)$ drawn from the DC bus is then calculated as the sum of the currents flowing through the upper switches of each inverter leg:

$$I_{dc}(t) = i_{S_{a+}}(t) + i_{S_{b+}}(t) + i_{S_{c+}}(t) \tag{2.14}$$

This represents the total current drawn from the DC source, as power is transferred between the DC side and the three-phase AC load.

2.1.5 Inverter Loss Modeling Methodology

Based on the previously computed three-phase inverter output currents, we proceed to estimate the inverter's internal power losses. These losses are primarily associated with the switching and conduction characteristics of the power semiconductor devices. The following section presents a detailed methodology for reconstructing the switching behavior and computing instantaneous power losses using datasheet-based interpolation and modulation signal analysis.

2.1.5.1 Overview

Accurate estimation of inverter power losses is critical for evaluating system efficiency, thermal management, and reliability. In this work, a physics-informed loss model is developed for a two-level voltage-source inverter employing silicon carbide (SiC) MOSFET devices. The model captures both conduction and switching losses, and is implemented in MATLAB using actual device characteristics obtained from manufacturer datasheets.

The model reconstructs the switching behavior of each power device based on the modulation strategy and calculates the instantaneous power losses as a function of time. The aim is to provide a time-resolved, device-level loss profile that can be used for thermal simulations and efficiency assessments.

2.1.5.2 Modulation and Switching State Reconstruction

The inverter is controlled using a sinusoidal pulse-width modulation (PWM) strategy with third harmonic injection (THIPWM). This technique modifies the reference voltage signals to increase the output voltage range and reduce harmonic distortion. The three-phase modulation signals are defined as follows:

$$\begin{aligned} v_{ma}(t) &= m\sin(\omega t) + \frac{m}{6}\sin(3\omega t), \\ v_{mb}(t) &= m\sin\left(\omega t - \frac{2\pi}{3}\right) + \frac{m}{6}\sin\left(3\omega t - 2\pi\right), \\ v_{mc}(t) &= m\sin\left(\omega t + \frac{2\pi}{3}\right) + \frac{m}{6}\sin\left(3\omega t + 2\pi\right), \end{aligned} \tag{2.15}$$

where m is the modulation index and $\omega = 2\pi f_m$ is the angular frequency of the fundamental component.

These continuous-time modulation signals are compared against a high-frequency triangular carrier waveform of frequency f_{sw} to generate initial binary gate signals for the inverter switches. To prevent shoot-through faults due to simultaneous conduction of upper and lower switches in the same inverter leg, a dead-time of 2 μs is inserted into each leg.

Based on this PWM logic with dead-time insertion, the switching status of each of the six MOSFETs (S_1 to S_6) is reconstructed at every simulation time step. Each switch is either in an ON (conducting) or OFF (non-conducting) state. Transitions

between these states correspond to switching events that cause additional switching energy losses.

2.1.5.3 Loss Model Formulation

The inverter loss model includes two primary components: conduction loss and switching loss.

- **Conduction loss:** When a switch is conducting current, its instantaneous conduction loss is calculated as

$$P_{\text{cond}}(t) = |I_{\text{sw}}(t)| \cdot V_{\text{on}}(I_{\text{sw}}, T_j),$$

  where $I_{\text{sw}}(t)$ is the instantaneous current through the device, and V_{on} is the on-state voltage drop obtained via interpolation from manufacturer-provided lookup tables as a function of current magnitude and junction temperature T_j. In this work, T_j is assumed to be constant at 25°C for simplification.
- **Switching loss:** When a switch transitions from OFF to ON or vice versa, it dissipates finite energy per switching event. The switching energy losses are given by

$$E_{\text{sw}} = E_{\text{on}}(I_{\text{sw}}, T_j) \quad \text{or} \quad E_{\text{off}}(I_{\text{sw}}, T_j),$$

  also obtained from datasheet-based lookup tables. The instantaneous switching power loss is computed by scaling the energy losses by the switching frequency and the instantaneous DC bus voltage:

$$P_{\text{sw}}(t) = f_{sw} \cdot (E_{\text{on}}(I_{\text{sw}}, T_j) + E_{\text{off}}(I_{\text{sw}}, T_j)) \cdot \frac{V_{\text{dc}}(t)}{V_{\text{ref}}},$$

  where V_{ref} is the reference voltage used in the datasheet measurements (e.g., 850 V), and $V_{\text{dc}}(t)$ is the instantaneous DC bus voltage.

The total instantaneous power loss of the inverter is obtained by summing the conduction and switching loss contributions over all six switches:

$$P_{\text{total}}(t) = \sum_{\text{devices}} \Big(P_{\text{cond}}(t) + P_{\text{sw}}(t) \Big).$$

2.1.5.4 Numerical Implementation

The loss model is fully implemented in MATLAB. The modulation waveforms are generated analytically, and PWM gate signals are produced via digital comparison with dead-time insertion. The switching states of the six inverter devices are reconstructed accordingly at a high sampling rate (1 MHz).

Three-phase output currents and the DC bus voltage are modeled as time-dependent inputs to the loss calculations. Device characteristics such as on-state voltage drop (V_{on}), turn-on energy (E_{on}), and turn-off energy (E_{off}) are extracted from manufacturer datasheets and interpolated via 1D linear interpolation functions at the fixed junction temperature of 25°C.

The model outputs a high-resolution, time-resolved loss power waveform $P_{\text{total}}(t)$ over the simulation duration (e.g., 0.1 s). This detailed loss profile enables further analysis for thermal management, efficiency evaluation, and inverter design optimization.

2.1.6 Result validation

Figure 2.3 demonstrates the loss results calculated using the methodology of this paper compared to the reference data. Although there are some errors, the predictions are still within acceptable limits. Therefore, the loss model has sufficient accuracy to be used as a heat source input in subsequent thermal simulations.

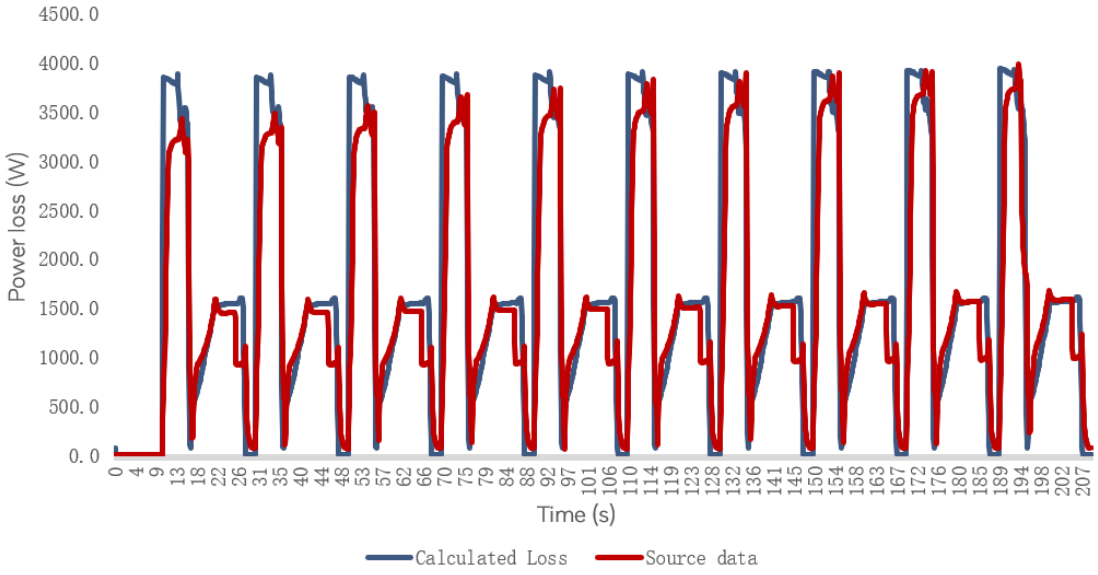

Figure 2.3: Comparison of power loss results: proposed method vs. reference data.

2.2 Working concept of PCM

Phase Change Materials (PCMs) are special materials, usually with a unique melting point, that are subject to a reversible phase change when the temperature reaches the melting point.

PCMs can absorb or release large amounts of latent heat during the phase change process while maintaining a nearly constant temperature. This property allows it to be used in thermal energy storage and temperature regulation applications. Figure 2.4 shows the typical temperature behaviour of a PCM. It shows that the PCM can absorb a large amount of heat during the phase transition, this heat is used to overcome the phase transition, the PCM maintains a constant temperature during the process.

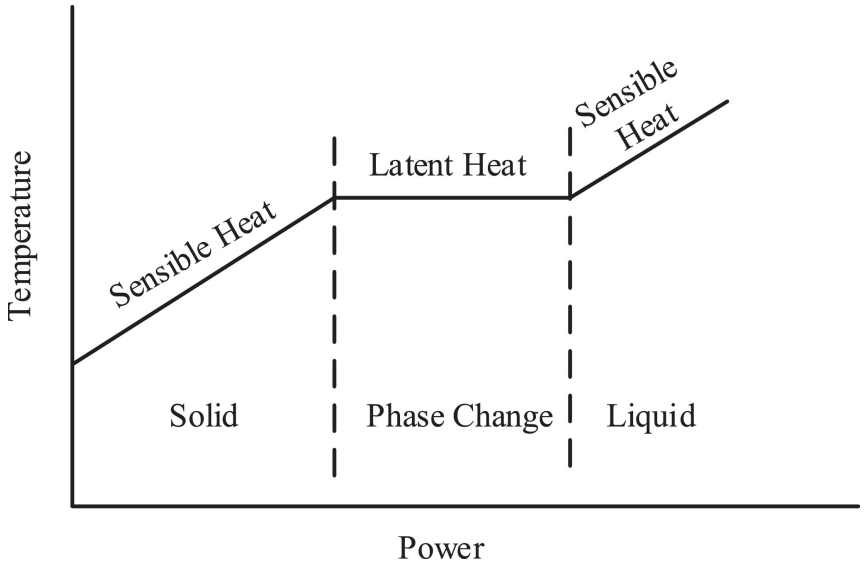

Figure 2.4: Typical PCM Temperature Characteristics

2.3 PCM materials and properties

In recent years, extensive research has been conducted on the thermal and physical properties of various PCMs. PCMs are generally classified into three major categories: inorganic,organic and eutectic materials. The selection of an appropriate PCM requires a comprehensive evaluation of several key factors, including its melting point, latent heat of fusion, density, thermal conductivity, and chemical stability. It is essential to ensure that the chosen PCM aligns with the specific thermal management requirements and operational conditions of the intended application to achieve optimal performance and reliability.

2.3.1 Organic PCMs

Organic PCMs often have a definite melting point, which can range from low to high temperatures, depending on their molecular structure. They have good nucleation behaviour, resulting in minimal or negligible subcooling effects during the phase change process. These characteristics contribute to their reliability and stability in thermal energy storage applications (Sharma et al., 2009). The following table shows some of the common organic phase change materials and their related parameters.

PCM	Melting temperature[°C]	Latent heat of fusion[kJ/kg]	Density [kg/m^3]	Thermal Conductivity [$W/m \cdot K$]	Refs
Caprylic acid	16.5	149	1033	No data	(Abhat, 1983)
Propylpalmitate(C17H34O2)	19	186	No data	No data	(Hasnain, 1998)
PEG600	22	127.2	1232	No data	(İbrahim Dinçer and Rosen, 2010)
ParaffinC13–C24	22-24	189	900	0.21	(Khudhair and Farid, 2004)
1-Iodehexadecane	22.2	131	No data	No data	(Babich, Hwang and Mounts, 1992)
n-Octadecane(C18H38)	28	244	814	0.358	(Abbas et al., 2019,Khudhair and Farid, 2004,Koschenz and Lehmann, 2004)
ParaffinC22–C45	58-60	189	920	0.21	(Khudhair and Farid, 2004)
n-Heptacosane(C27H56)	58.8	235	No data	No data	(Pielichowska and Pielichowski, 2014,Abdul Hussain Ayash, 2019)
Palmiticacid	60-61	197.9	942	No data	(Sarı and Kaygusuz, 2003,Sari and Kaygusuz, 2002)

Table 2.1: Thermal and physical properties of various organic PCMs. Data compiled from multiple sources (Abhat, 1983; Hasnain, 1998; Babich, Hwang and Mounts, 1992; Khudhair and Farid, 2004; İbrahim Dinçer and Rosen, 2010; Abbas et al., 2019; Koschenz and Lehmann, 2004; Pielichowska and Pielichowski, 2014; Abdul Hussain Ayash, 2019; Sarı and Kaygusuz, 2003; Sari and Kaygusuz, 2002). Specific references are provided in the table.

2.3.2 Inorganic PCMs

Inorganic phase change materials consist mainly of salt hydrates and metal alloys. Salt hydrates have a fixed melting point, a high latent heat, and a low cost. However, their practical application often encounters difficulties such as inconsistent melting, which can result in density gradients, settling and phase separation during repeated phase change cycles. These problems can adversely affect the long-term thermal reliability and stability of the material (Cabeza et al., 2003).
Metal alloys tend to have high melting points and are therefore commonly used in high temperature thermal storage applications. In addition to their high melting points, these alloys exhibit excellent stability and thermal reliability (Liu, Saman and Bruno, 2012). Among them, binary and ternary alloys consisting of elements such as aluminium, copper, magnesium and zinc have the highest latent heat, both by mass and by volume. However, it is worth noting that not all combinations of these elements are suitable for use as phase change materials, as various combinations differ in their phase change behaviour, thermal stability and compatibility with specific applications and require careful analysis (Scopus.com, 2025)

2.3.3 Eutectics

Eutectic systems are homogeneous mixtures of two or more components, each with its own melting point, which, when mixed in specific proportions, exhibit a single, sharp melting and solidification point. This property ensures that eutectic mixtures typically undergo phase transitions simultaneously, behaving like a single substance during melting and solidification. Eutectic materials can be classified as organic-organic systems, inorganic-inorganic systems or organic-inorganic systems (Hasnain, 1998). One of the main advantages of eutectic phase change materials is the ability to adjust the melting temperature and latent heat value by selecting the appropriate component materials and adjusting the composition ratio, thus allowing precise control of the thermal properties to meet specific application requirements (Singh et al., 2021).

2.3.4 PCM selection and use

Several key factors must be systematically evaluated in the use of PCMs to enhance the thermal management performance of automotive inverters. These factors include selecting PCMs with melting points that match the inverter's operating temperature range to ensure effective heat absorption and release under normal and peak load conditions. In addition, the material must have excellent thermal reliability and cycling stability, maintaining consistent phase change behaviour and thermal properties over multiple heating and cooling cycles.
In addition to thermal performance, practical considerations such as ease of material processing and fabrication, availability of raw materials, and overall cost of production and system integration need to be taken into account to ensure economic viability. Other key factors include the thermal conductivity of the PCM (which directly affects the rate of heat transfer); chemical stability (to prevent material degradation over time); compatibility with encapsulation materials; and safety aspects such as flammability and potential toxicity.

2.4 Thermal Conductivity Enhancer(TCE)

A major disadvantage of PCM is that PCM itself has a low thermal conductivity, usually only about 0.5. This results in PCM that is close to a heat source being able to absorb heat and melt, while PCM that is far from the heat source is not able to function. Therefore, it is important to find ways to increase the thermal conductivity of PCM.

2.4.1 Fin

Of all the methods, the use of highly thermally conductive fins is perhaps the simplest and most straightforward (Wang, Zhang and Xia, 2017). The incorporation of thermally conductive fins establishes enhanced heat transfer paths in phase change material (PCM) systems, facilitating the directional diffusion of heat to the distal region through its extended surface structure. The fin-enhanced thermal network compensates for the molecular-level thermal resistance properties of organic phase change materials through macro-geometry optimisation, demonstrating a synergistic approach to thermal management system design. When using fins, factors such as their shape, size, quantity, and assembly with the PCM need to be considered. Figure 2.5 shows the structure of a typical fin.

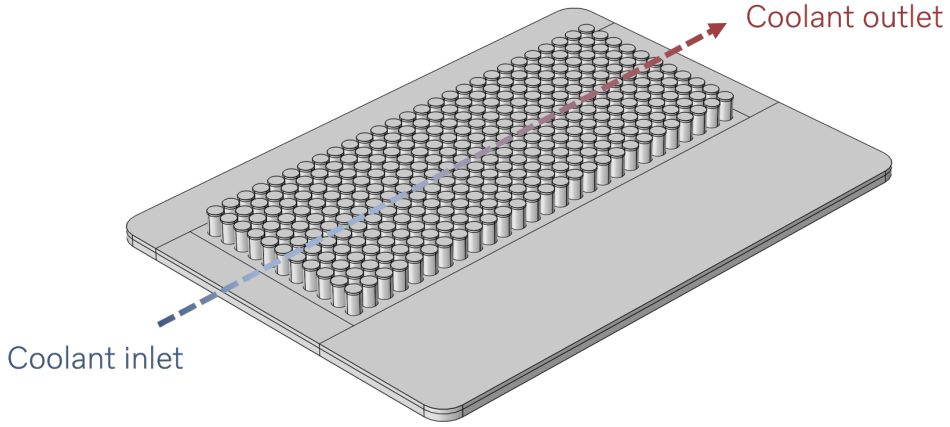

Figure 2.5: Schematic diagram of the fin

Weng et al. (Weng et al., 2019) studied various PCM-fin systems. They found that the temperature of the system was lower when using the branch fin structure as compared to the conventional fin structure, and among all twelve fin structures, the X-shaped fin had the best results.Sharma et al. (Sharma et al., 2019) (Sharma, Agarwal and Prabhakar, 2023) investigated twelve different fin designs and compared them with two benchmark cases without fins. They found that two fin designs exhibited different thermal performance than before when the PCM volume fraction was the same. Liu et al. (Liu et al., 2023) designed and optimised an enhanced hybrid cooling system with an integrated PCM and liquid-cooled fin in order to be used under long-term cycling.Kalapala et al. (Influence of operational and design parameters on the performance of a PCM based heat exchanger for thermal energy storage – A review, 2018) focused on various operational and design factors to improve the thermal performance of PCM-HEX. According to their findings, the geometrical orientation of the heat transfer fluid (HTF), the temperature and mass flow rate, the tube structure, and the arrangement and sizing of the fins all have an impact on the results.

2.4.2 Nanocomposite

Addition of conductive nanoparticles to PCM enhances its thermal conductivity. Suresh Kumar and Kalaiselvam investigated the effect of addition of copper oxide nanoparticles to palmitic acid on its thermal properties (Suresh Kumar and Kalaiselvam, 2017).P. Manoj Kumar et al., 2023) investigated the effect of MgO nanoparticles on the thermal properties of inorganic PCM and the results showed that the thermal conductivity increased to 0.902 W/mK when the concentration of MgO NP was 0.75 per cent.Kalidasan et al. (P. Manoj Kumar et al., 2023) investigated the effect of MgO nanoparticles on the thermal properties of inorganic PCM. The results showed that the thermal conductivity increased to 0.902 W/mK at 0.75% MgO NP concentration. (B Kalidasan et al., 2023) investigated the synergistic effect of carbon nanoparticles with polyethylene glycol to improve the thermal conductivity and performance of the energy storage device. Lin and Al-Kayiem (Lin and Al-Kayiem, 2016) investigated the effect of the embedded paraffin wax the effect of the number

of copper nanoparticles on the thermal properties of paraffin wax. The thermal conductivity increased by 14.0%, 23.9%, 42.5% and 46.3% when paraffin wax contained 0.5 to 2.0 %wt of copper nanoparticles.Narayanan et al. (Narayanan et al., 2017) investigated a nanocomposite PCM consisting of a eutectic gel and 0.5 wt% of graphite nanoparticles. The nanocomposite PCM was encapsulated in a copper block in a copper block and then wrapped with a copper coil cable.

2.4.3 Metal Foam

Metal foam is a hollow material with many internal pores, consisting of a metal matrix filled with a large number of connected or closed pores. Due to this special structure, it has good thermal conductivity, high specific surface area and excellent mechanical properties. Metal foams are widely used in thermal management, energy absorption and cushioning, and structural weight reduction. Figure 2.6 shows a two-dimensional schematic of a metal foam, which shows that there are many pores distributed in the structure.

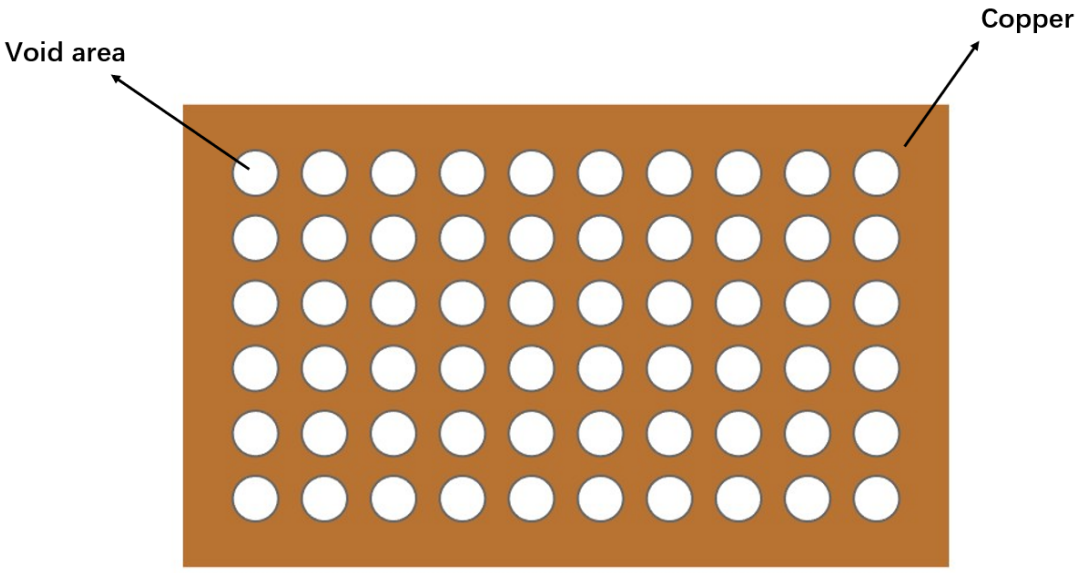

Figure 2.6: Schematic diagram of metal foam structure

Porosity is a key parameter describing the internal porosity of the metal foam material, which indicates the proportion of the pore volume to the total volume, and is an important index for judging the performance of the material in terms of air permeability, thermal conductivity, adsorption capacity and so on. Its expression is as follows.

$$\phi = \frac{V_{\text{void}}}{V_{\text{total}}} = 1 - \frac{V_{\text{solid}}}{V_{\text{total}}} \tag{2.16}$$

Buonomo et al. (Buonomo et al., 2022) investigated the effect of adding a metal foam layer on the tube on the thermal performance of a shell-and-tube LHTES device, and showed that increasing the thickness of the foam layer reduces the melting time. Zhu et al. (Zhu et al., 2018) investigated the effect of the porosity of 96% and

different pore densities (15 PPI and 30 PPI) on the thermal performance of heat-sink-transient output of PCM and copper foams. Joshi and Rathod (Joshi and Rathod, 2019) numerically investigated the effect of fill rate and foam porosity on the thermal performance of PCM and found that only the lowest fill rate (0.25 of the height) improved the thermal efficiency. In the unfilled metal foam and full volume metal foam configurations, the melting rate was 1.87 and 1.25 times faster at a porosity of 95%, respectively. Marri and Balaji (Marri and Balaji, 2021) combined numerical and experimental approaches to investigate the thermal performance of aluminium foams with different PPIs, porosities, and n-octacosane, the phase change material. The results show that decreasing the porosity or increasing the PPI has a better effect on the thermal efficiency of the heat sink than the case of uniform PPI and porosity.Iasiello et al. (Iasiello et al., 2021) reported simulation and experimental results investigating the effect of aluminium-metal foams on the performance of PCMs with different orientations, porosities, PPIs, and heat flow densities. The results showed that the lower the porosity, the higher the melting fraction, while PPI and orientation had no relevant effect on the melting time. Diani and Rossetto (Diani and Rossetto, 2021) investigated the effect of copper foams with different porosities on the melting of PCM at different melting temperatures (e.g., 42, 55, and 64 °C), and the results showed that the 90.5% porosity of the Copper foam with a porosity of 93.3% performed slightly better than that with a porosity of 93.3%.Li et al. (Li et al., 2012). It was shown that lowering the PPI can improve the temperature uniformity of saturated paraffin in copper foam, as well as lowering the porosity or increasing the natural convection, thus increasing the effective thermal conductivity. Mancin et al. (Mancin et al., 2015) investigated the embedding of copper foam in PCMs with three different melting points, and found that the copper foam acted as a heat sink, resulting in a more uniform temperature distribution and a PCM phase change faster.

3

Methods

3.1 Geometry design

Figure 3.1 shows a schematic diagram of the various structures in the radiator and the schematic diagram of the cooling system associated with it.

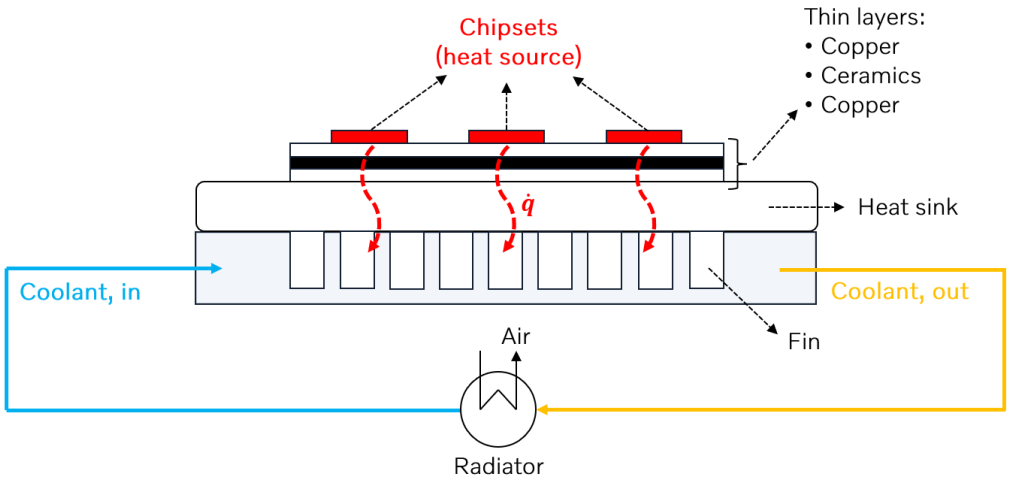

Figure 3.1: Cooling system and radiator schematic

In our application we needed to optimise an existing radiator. Since the power section of a modern electric car is very compact, we didn't have much room to add additional structure, so using metal foam became the best option for us. We placed the metal foam and the PCM integrated cooling system in the part of the original radiator above the fins. The picture below shows a three-view of the model used.

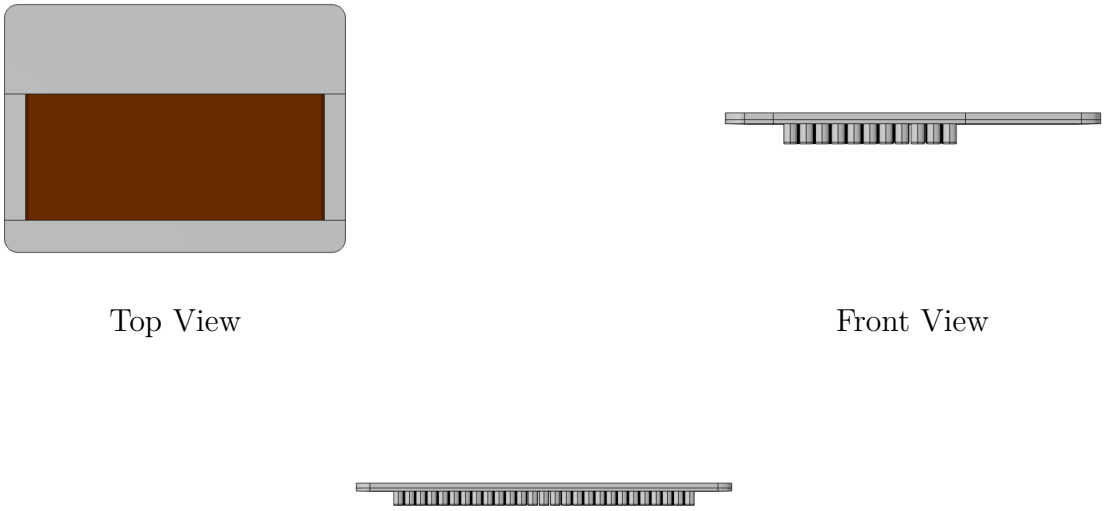

Top View

Front View

Side View

Figure 3.2: The three views of the model

In the model, the brown part represents the PCM+MF area, and the rest is the original configuration of the radiator, which has not been changed.

3.2 Numerical procedure and model validation

3.2.1 PCM and MF

In this simulation, the PCM we used is RT70HC from RUBITHERM, and its specific parameters are shown in the following table 3.1

Parameter name	Numeric	Unit
Melting area	69-71	℃
Heat storage capacity	260	KJ/Kg
Density solid	0.9	Kg/L
Density liquid	0.8	Kg/L
Heat conductivity (both phases)	0.2	$W/(m \cdot K)$

Table 3.1: Parameters of the PCM used

The melting point of this PCM is close to 70°C, which is close to the temperature at which the chip on the inverter operates normally. In this simulation, copper foam is used, which has a relatively high thermal conductivity, which helps us improve the thermal conductivity of the entire heat dissipation system.

3.2.2 Coolant

The coolant used in this simulation is from Volvo Cars and its specific parameters are shown in Table 3.2. This coolant will maintain a constant flow rate, which is shown in table 3.2. The typical flow rate of the coolant in the inverter cooling system of an BEV under real working conditions is about 15 L/min. In order to better investigate the role of the PCM in passive thermal management, the coolant flow rate in the simulation is set to 0.5 L/min. The purpose of using this setting is to amplify the dominant role of the PCM in the response to the thermal loads, and to reduce the effect of active cooling on the results. This setting can provide a clearer physical context for structural optimisation and parametric analysis.

Parameter	Value	Unit
Heat capacity	3470	$J/kg \cdot K$
Density	1126	kg/m^3
Thermal conductivity	0.38	$W/m \cdot K$

Table 3.2: Coolant parameters

3.2.3 Numerical simulation methods

The simulation was performed using the finite element analysis software Comsol Multiphysics 6.2. To simulate the energy transfer behavior of the solid-liquid interface during the phase change process, this paper uses a phase change model based on the Heaviside function. The advantages of this method are that it avoids explicitly tracking the phase interface and achieves a smooth transition of the solid-liquid phase change process. By using the Heaviside function, we can effectively bring the latent heat effect into the energy equation, which increases the numerical stability and improves the simulation accuracy, so it is suitable for solving complex geometric structures and unsteady heat transfer problems. In COMSOL, the mathematical expression of Heaviside function is:

$$H(T) = \frac{1}{2}\left[1 + \tanh\left(\frac{T - T_m}{\delta T}\right)\right] \tag{3.1}$$

Where:

- T: Current temperature;
- T_m: Melting point (or phase change temperature);
- δT: Smoothing factor (transition width, controlling the steepness of the phase change transition);
- tanh is the hyperbolic tangent function, used to achieve a smooth transition.

Thermal properties, including density, specific heat, thermal conductivity, and latent heat, are defined as constant to reduce simulation pressure.

3.2.4 Mesh and time step independent test

For the grid independence analysis, we considered three different grids: coarse grid (117975 elements), normal grid (242052 elements) and fine grid (582233 elements),

with a time step of 1s to reduce its impact on the simulation accuracy. Table 3.3 lists the results of the average operating temperature under three grid conditions when the calculation time is t = 30s.

Number of elements	Temperature(°C)	Deviation(%)
117975	66.74	2.7%
242052	69.65	1.5%
582233	68.61	0%

Table 3.3: Results dependence on grid size variations

The maximum variation of the operating temperature is only 1.5%, which is negligible when the grid number is 242,052 and 582,233. Therefore, choosing a grid with a cell number of 242,052 reduces the computation time while maintaining the accuracy of the solution.
In order to assess the independence of time steps, simulations were performed with three different time steps (0.1 s, 0.5 s and 1 s) based on 242,052 grids. The results for the 1 s time step were used as a reference. The results show that the average temperature deviation of the inverter at 0.1 s and 0.5 s time steps is only 0.42% and 0.22% with respect to that at 1 s, which is so small that it is negligible. Therefore, the combination of 242,052 grids and 1 s time step was chosen for this study as it provides a good balance between computational accuracy and efficiency.

Time steps	Temperature(°C)	Deviation(%)
0.1	69.94	0.42%
0.5	69.80	0.22%
1.0	69.65	0%

Table 3.4: Results dependence on time step variations

3.3 Hypothesis

The following assumptions are made in the simulation model:

(a) The PCM used is a homogeneous material with the addition of nanoparticles, also known as NePCM. its phase transition temperature varies over a range of 10 °C.

(b) The flow of liquid PCM inside the MF is considered to be two-dimensional, Newtonian, laminar, transient, and incompressible. This simplifies the Navier-Stokes equations and is commonly used for modeling thermal systems. However, it may ignore three-dimensional flow effects and turbulence at high flow rates.

(c) All open-cell metal foam materials are assumed to be homogeneous and isotropic.Although actual foams may have anisotropic structures, this assumption reduces computational costs and is widely used. It may introduce small deviations in

directional thermal conductivity.

(d) The thermophysical properties of the substrate and the metal foam are assumed to be constant. This is standard in many simulations, although temperature-dependent properties at larger gradients can produce more accurate results.

(e) Except for the density of the PCM, all thermophysical properties of both the PCM and the NePCM are assumed to be constant in each phase.

(f) The initial temperature of the PCM, substrate, and metal foam is uniformly set to 45 °C. Initially, the PCM is entirely in the solid phase.

(g) The coolant enters at a constant temperature of 45 °C with a fixed flow rate of 0.5 L/min.

(h) Local thermal equilibrium is assumed between the metal foam and the PCM, implying no slip or temperature difference between them.

3.4 Validation of the numerical model

Since the research problem involves a complex mechanism, a comprehensive validation study is required to ensure the reliability of the numerical model developed in this paper. To this end, several validations have been carried out, including heat transfer validation and PCM phase transition process validation.

3.4.1 Heat Transfer Validation

Firstly, after building the whole cooling plate model, we verified it without adding PCM, focusing on verifying that the material properties, meshing and heat transfer are correct. We compared the model with Volvo's experimentally validated simulation model from the Star-CCM+ and after using the same heat source, the comparison results are shown below.

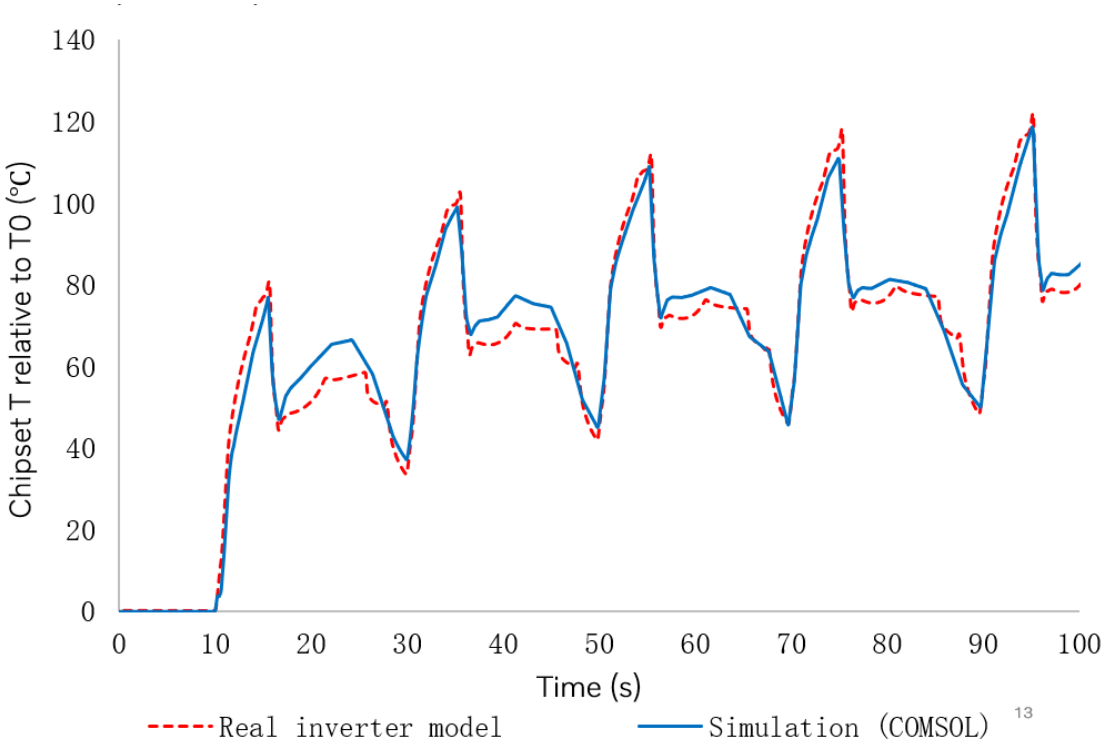

Figure 3.3: Heat transfer results validation

From the results, it can be seen that the model used in this paper has acceptable consistency with the reference model, which indicates that this model can be used for subsequent research

3.4.2 PCM model simulation validation

After confirming that the basic heat transfer model is correct, it is necessary to validate the treatment of the PCM in the model of this paper. For this purpose, a numerical model incorporating the PCM was developed and compared and validated with the actual experimental results of Rehman and Park. (Rehman and Park, 2024), as shown in Figure 3.4.

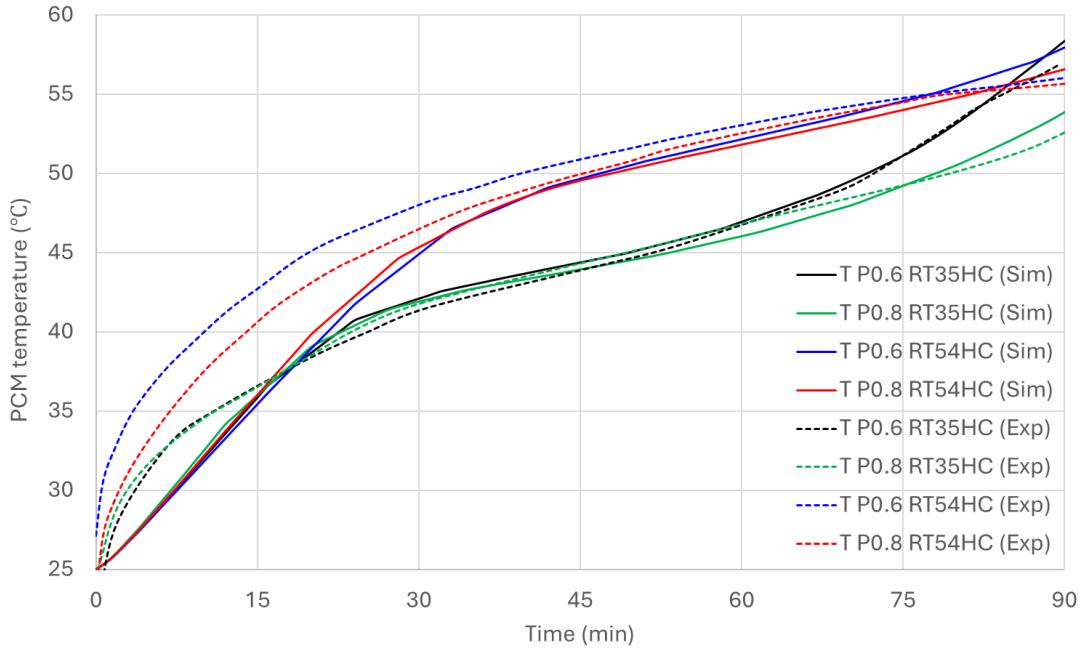

Figure 3.4: Comparison chart with the results of Rehman and Park

From the figure, we can see that our simulation results are basically consistent with their experimental results, which indicates that our modelling parameter settings for the PCM in this paper are reasonable. The consistency of the two results can also further verify the physical accuracy of the thermal management model constructed in this paper and the credibility of the simulation results.

4

Results and discussion

Our main goal is to reduce or slow down the temperature change of the on-board inverter as much as possible and keep its temperature within the allowable limit. To this end, this study explores the comprehensive impact of integrating PCM on the inverter temperature in the heat dissipation model mentioned above. The melting process, temperature distribution, and liquid fraction of the basic PCM, PCM+MF, and the new design using PCM+MF are studied.

4.1 The effect of PCM

What we hope is to use PCM to absorb the heat generated by the on-board inverter whenever there is a sudden heat generation in inverter to achieve the effect of stabilizing the temperature. The first thing to do is to verify whether PCM has such a function.

4.1.1 The effect of PCM in simple model

The PCM is integrated into the simulation model shown in Figure 4.1. In this model, the hole area is filled with PCM, and the rest of the structure is made of copper. A heat source with a constant power of 100 W is applied to the bottom of the model, and the thermal response of the system is simulated for 100 s. Figure 4.2 shows the temperature change trend of the bottom of the model during this period.

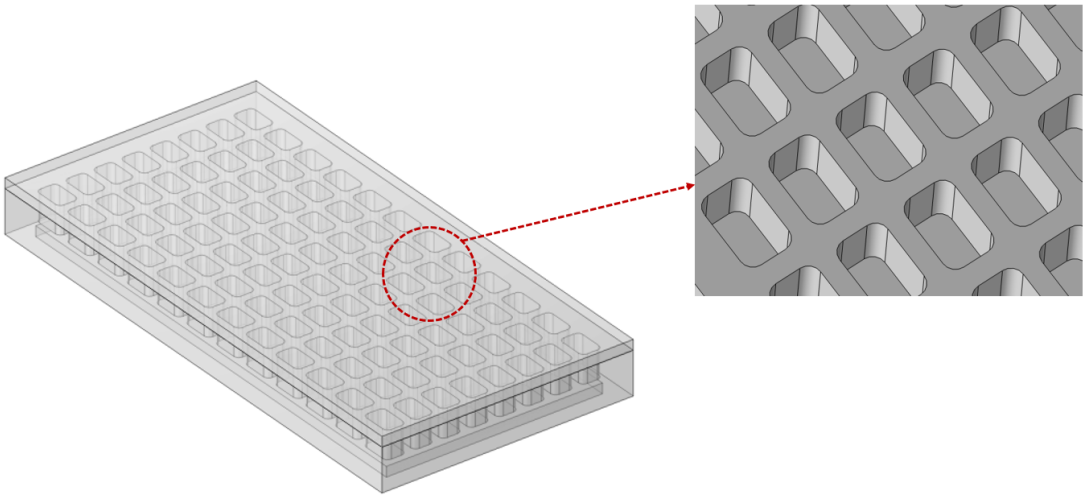

Figure 4.1: Model diagram

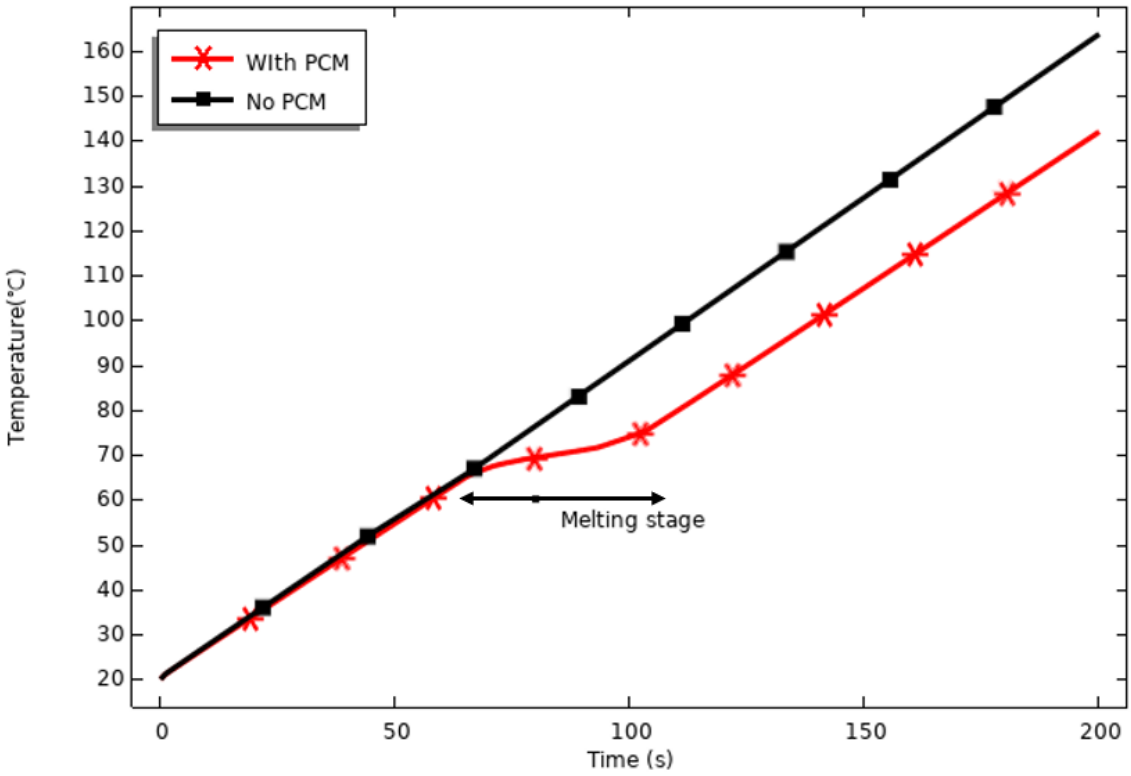

Figure 4.2: Temperature response curve over time

As can be observed from Figure 4.2, when the temperature reaches the melting point of PCM, PCM begins to undergo phase change. At this stage, the temperature rise rate of the target area slows down significantly and tends to be stable. This shows that PCM maintains a nearly constant temperature while absorbing heat, reflecting its latent heat absorption characteristics and verifying its expected temperature control effect in thermal management.

4.1.2 The effet of PCM configuration in the real geometry

After verifying the thermal regulation effect of the phase change material PCM in the simplified model, this study further integrated the PCM into the original heat sink structure and applied the time-varying heat source mentioned above to simulate the actual working conditions,figure 4.3 shows how the PCM is integrated in the heat sink,the blue part is the PCM.In the simulation, the coolant flows continuously from the lower left side to the right with an initial temperature of 45°C. At the same time, the MOSFET heat source is located at the top of the structure, and the heat is conducted downward in the vertical direction. The research focuses on the temperature response of the heat source area (i.e., the location of the MOSFET chip). In order to evaluate the thermal management performance of PCM, the thermal responses of the two heat sink structures with and without integrated PCM under the same working conditions were compared and analyzed, and the relevant results are shown in Figure 4.4.

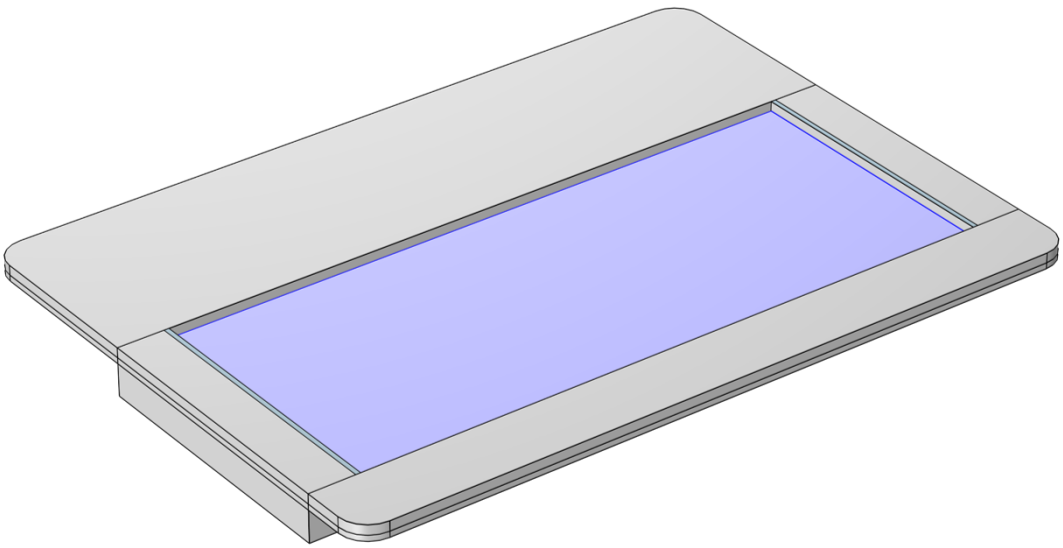

Figure 4.3: Heat sink with integrated PCM

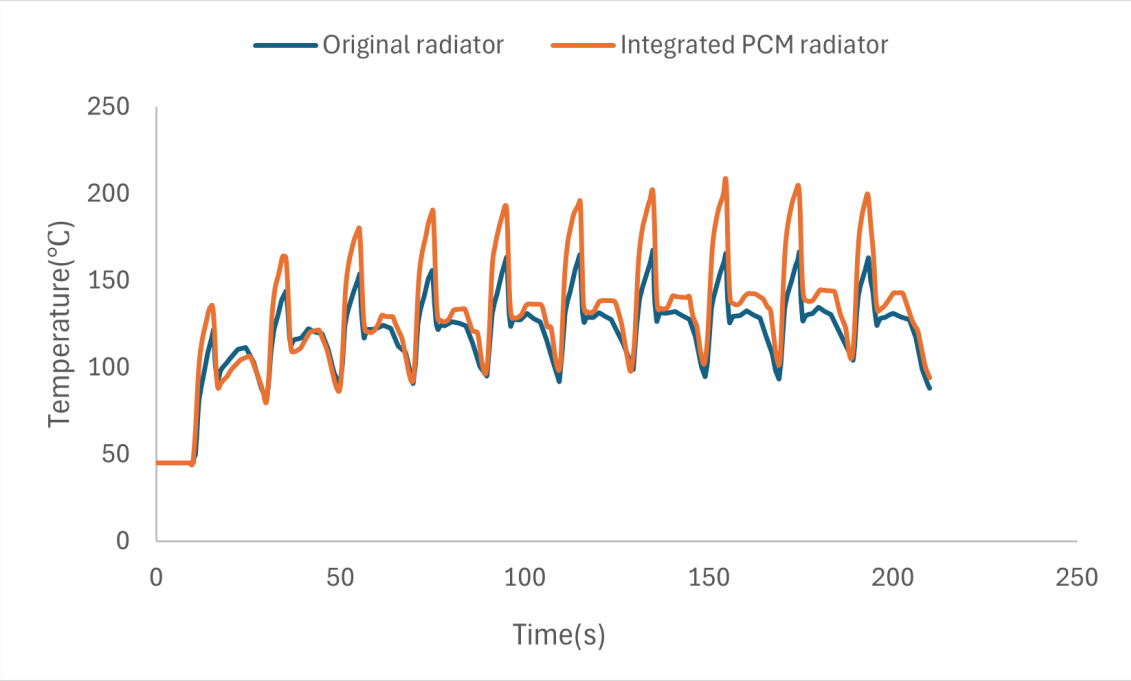

Figure 4.4: Comparison of MOSFET temperature with and without PCM-enhanced radiator

However, it can be observed from the results in Figure 4.3 that the temperature of the heat sink with integrated PCM in the MOSFET area is higher than that of the original heat sink without integrated PCM, which is obviously different from the expected cooling effect. Preliminary analysis shows that this phenomenon may be attributed to multiple factors. First, the thermal conductivity of the selected PCM material is low, only 1 $W/(m \cdot K)$, which limits its heat absorption capacity in the early stage of the heat source operation and significantly inhibits the effective conduction of heat to the coolant area. Secondly, the volume of the PCM in the model is relatively small, and its latent heat capacity is limited, which cannot absorb enough heat to significantly reduce the chip temperature. At the same time, due to the continuous heat input, the PCM failed to re-solidify in time after melting, and thus could not achieve the multi-cycle thermal regulation function. These factors together led to the overall thermal management performance not meeting expectations. In order to further reveal the thermodynamic mechanism of the phenomenon, this paper will show 3D simulation results from COMSOL of the temperature field inside the heat sink and the phase transition at critical moments to visually compare the thermal conductivity characteristics of the PCM and its effect on the thermal behavior of the system.

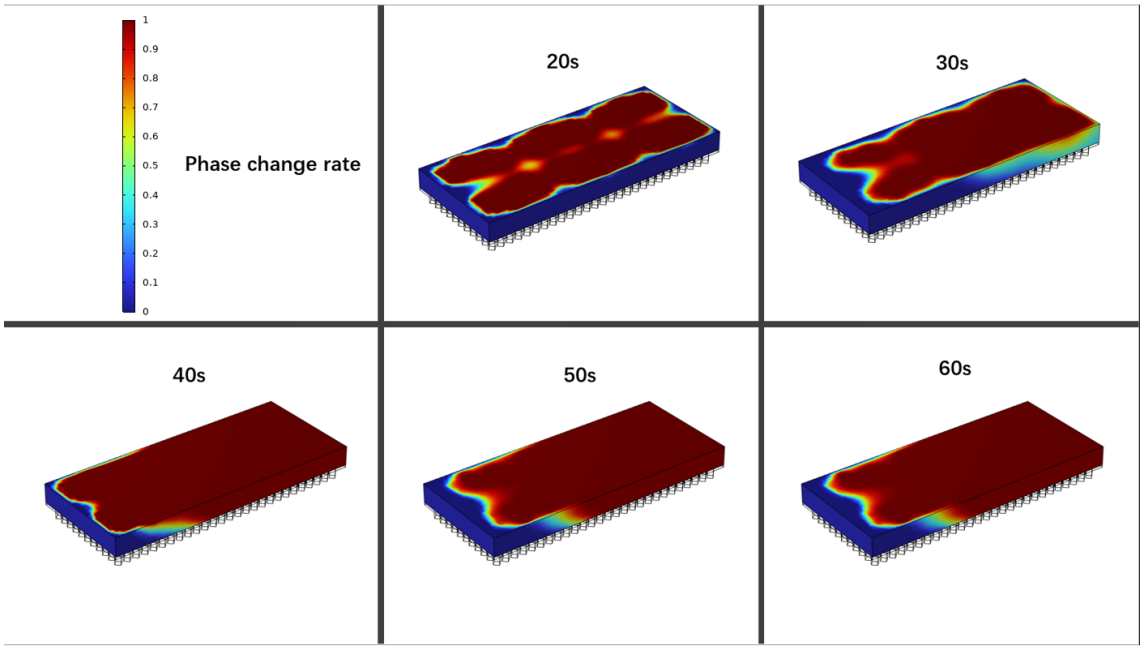

Figure 4.5: Phase change rate at different times

It can be observed from Figure 4.5 that the PCM near the heat source area undergoes phase change first, which indicates that heat conduction starts rapidly in the local area. However, due to the continuous flow of coolant, there are obvious differences in the degree of melting of PCM at different locations. Especially near the coolant inlet, only the PCM close to the heat source melts, while the PCM located below and directly in contact with the coolant is always maintained in a solid state due to continuous cooling, and fails to effectively participate in the heat absorption process, resulting in a waste of thermal management resources. In contrast, in the area far from the coolant inlet, the PCM is basically completely melted within tens of seconds, showing a strong local heat absorption ability. In addition, it can be observed that in the gap between the two driving cycles (such as the 20th and 30th seconds), some PCM re-solidifies. This phenomenon is mainly attributed to the decrease in heat source power during the vehicle deceleration stage, and the coolant takes away part of the accumulated heat, causing the PCM temperature to drop below the phase change temperature, thereby undergoing a phase change back to the solid state. This process reveals the reversible heat storage capacity of PCM under dynamic heat load, which is of great significance for the optimization of subsequent thermal management strategies.

4.2 The effect of metal foam

Based on the previous analyses, it was decided to use metal foam in this paper. The metal foam is characterised by high specific surface area and high thermal conductivity, which can significantly increase the effective thermal conductivity of the PCM region while maintaining a low volume increment. Its porous structure helps to accelerate the diffusion of heat inside the PCM, thereby enhancing the heat ex-

change efficiency during the phase change process. In addition, metal foam can also improve the uniformity of temperature distribution inside the PCM to a certain extent, reduce local overheating, and help the system maintain a stable thermal state. Figure 4.6 shows the simulation results after integrating the PCM+MF composite structure into the original radiator structure, and compares the temperature distribution without metal foam to further evaluate its thermal regulation performance under dynamic heat load conditions.

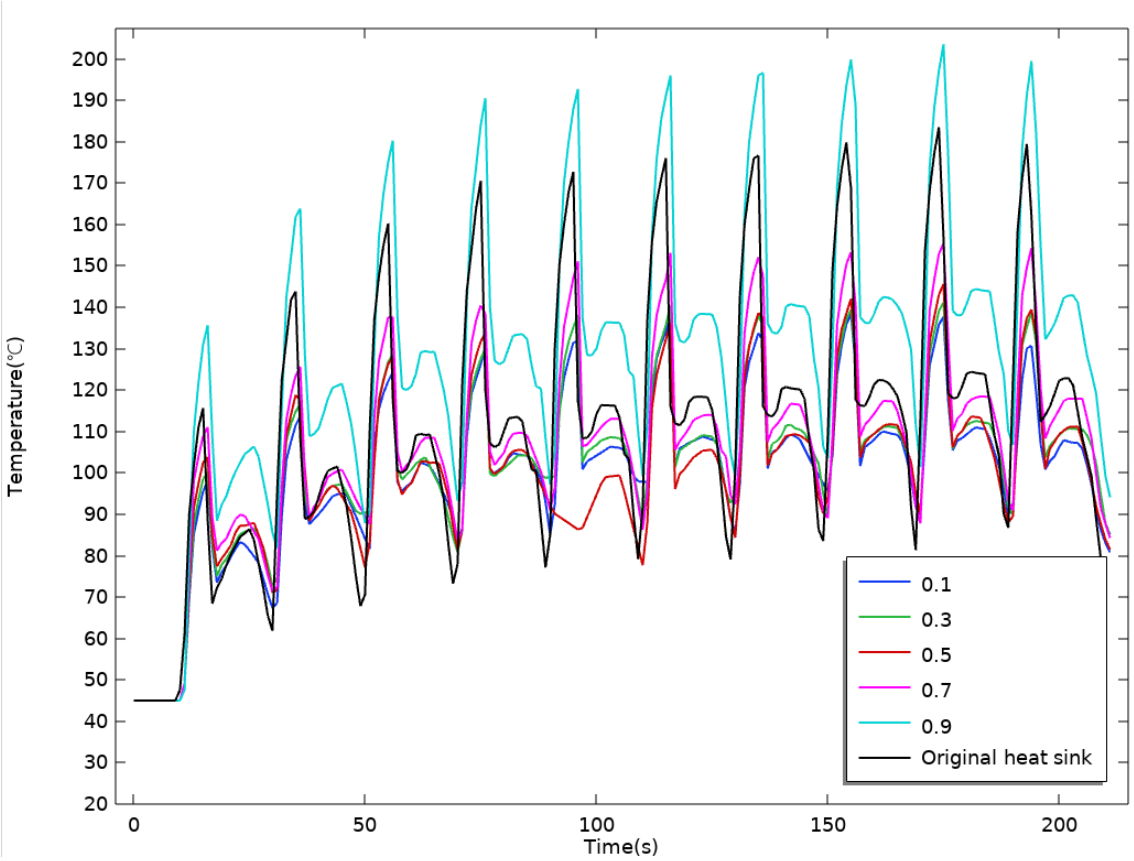

Figure 4.6: MOSFET temperature variation under different metal foam porosities

As can be seen in Figure 4.6, there is a significant difference in the effect of metal foams with different porosities on the MOSFET heat source temperature. Overall, all groups show better results compared to the original heat sink, except for the case with a porosity of 0.9. In particular, in the fifth driving cycle, the metal foam with a porosity of 0.5 can be seen to have significantly lower temperatures compared to the other groups, and a trend towards constant temperatures is seen. This shows that medium porosity has achieved a better balance between thermal conductivity and heat storage capacity. In the case of a porosity of 0.9, its overall thermal conductivity is low, and the metal skeleton accounts for a small proportion, making it difficult to effectively export heat from the heat source area, resulting in a decrease in overall heat dissipation performance. However, it is worth noting that in the deceleration stage of the first two driving cycles, the structure with a porosity of 0.9 is better than the original radiator in short-term temperature performance. This may be because when the heat source power decreases during the deceleration stage, the

structure can use the latent heat absorption of PCM to delay the temperature rise, and form a temporary "insulation" effect due to its low thermal conductivity.

In addition, it can be found from the figure that the temperature curve tends to be stable for a certain period of time during the deceleration phase of each driving cycle, which is the second peak part. This phenomenon indicates that the heat transfer and phase transition rate of the metal foam-PCM composite structure reached a dynamic equilibrium under the significantly reduced heat input, which made the system temperature temporarily maintained near the PCM phase transition plateau. This property is of positive significance for suppressing the peak temperature fluctuation and improving the thermal stability of the system.

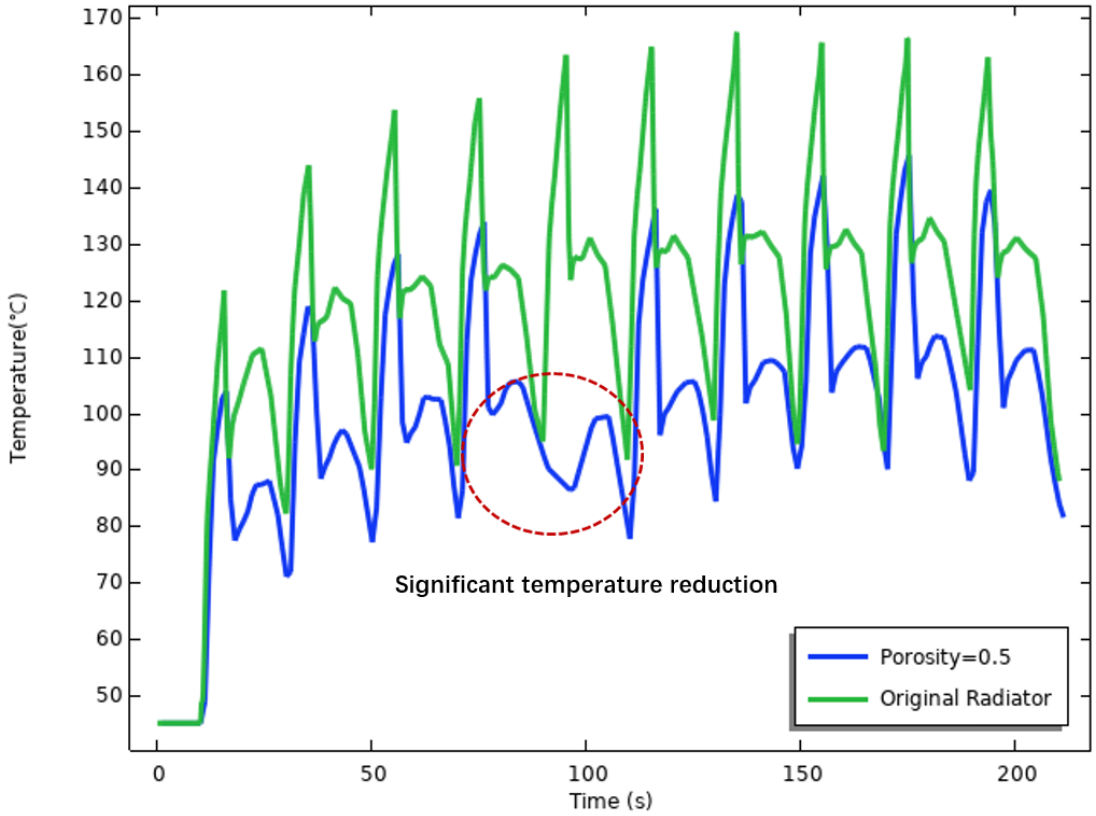

Figure 4.7: Temperature at porosity 0.5

Figure 4.7 shows the time trend of the MOSFET heat source temperature in the composite structure of the original heat sink and the integrated metal foam with a porosity of 0.5 under the driving cycle condition. It can be observed that the temperature of the structure after the integration of metal foam is significantly lower than that of the original heat sink without metal foam added during the entire simulation period, and the peak temperature is significantly reduced, and the overall temperature fluctuation amplitude is reduced, showing better thermal management performance.

This phenomenon can be attributed to the high thermal conductivity skeleton of

the metal foam, which effectively improves the thermal conductivity of the PCM area, allowing heat to diffuse more quickly in the phase change material, and is also conducive to improving the thermal utilization of the PCM. Compared with the previous structure without the addition of metal foam, this structure can more efficiently conduct the heat generated in the MOSFET area to the cooling medium contact area, thereby reducing the accumulation of heat around the chip. In addition, the three-dimensional interconnected structure of the metal foam also improves the temperature distribution inside the PCM, making it closer to uniform, which helps the continuous phase change process and suppresses local overheating.

From the curve fluctuation shape, each peak-valley cycle in the figure corresponds to a typical acceleration-deceleration process, and the temperature drop rate in the deceleration stage is faster and smoother in the structure of integrated metal foam, indicating that the structure has better responsiveness and thermal buffering capacity under dynamic heat load changes. Especially after the fifth cycle, the temperature suppression effect is more obvious, which may be related to the fact that the PCM has partially melted in the early stage and entered the heat capacity platform range.

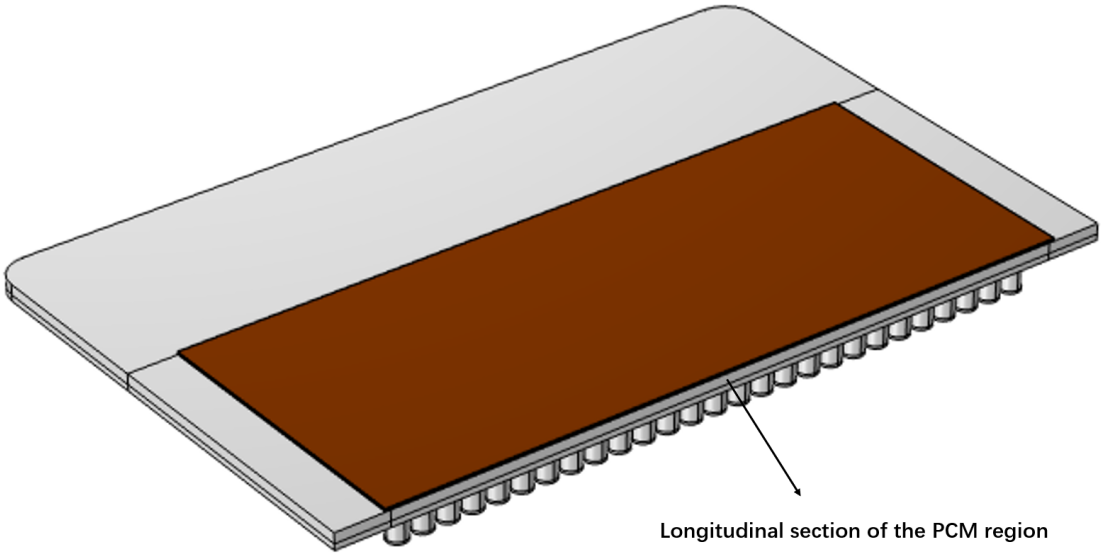

Figure 4.8: Longitudinal section of the MOSFET region

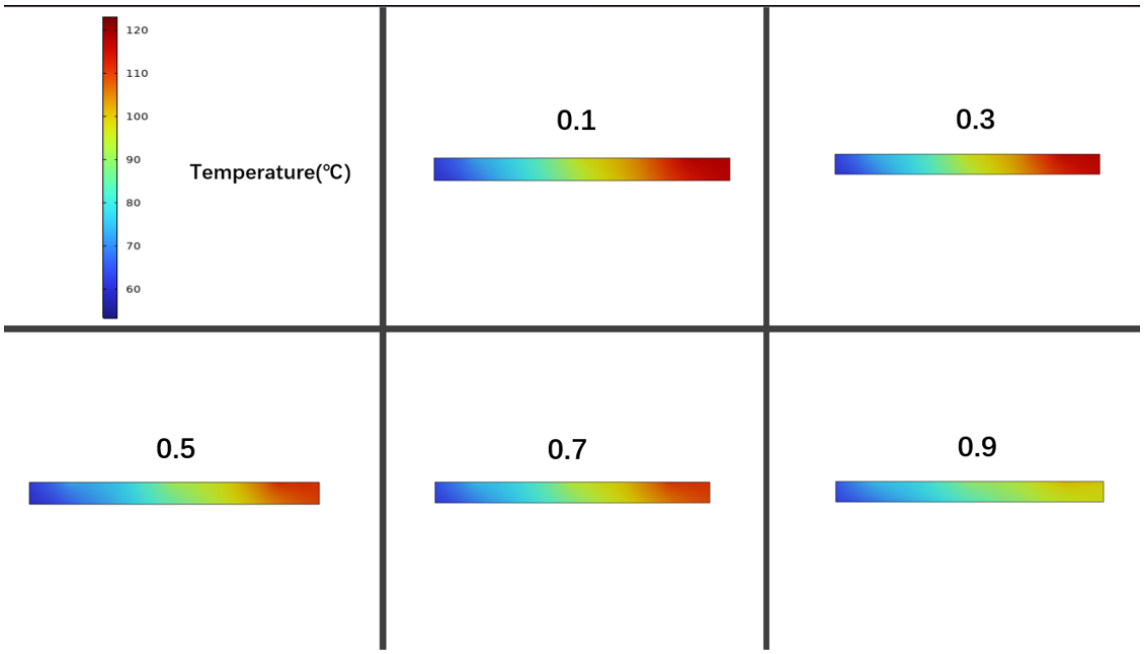

Figure 4.9: Temperature distribution at t = 100 s along the longitudinal section of the MOSFET region for PCM/metal foam composites with different porosities

Figure 4.9 shows the effect of different metal foam porosities (0.1, 0.3, 0.5, 0.7 and 0.9) on the temperature distribution of the PCM+MF composite structure under the same heat source and boundary conditions. The figure shows the temperature field distribution results along the longitudinal section of the MOSFET area at t = 100 s.

It can be observed that when the porosity is low (such as 0.1 and 0.3), the overall temperature level is significantly higher and the high temperature area is larger. This is mainly due to the high proportion of solid skeletons in metal foams. Although they have high thermal conductivity, the volume fraction of PCM they contain is small, resulting in limited phase change heat absorption capacity and difficulty in fully alleviating the temperature rise generated by the heat source. When the porosity is 0.5 and 0.7, the temperature field is more uniform as a whole and the high temperature area is reduced, indicating that the porosity within this range achieves a good trade-off between thermal conductivity and heat storage capacity, thereby improving the overall heat dissipation efficiency.

When the porosity is further increased to 0.9, although the volume of PCM increases, the proportion of metal skeleton decreases significantly, and the effective thermal conductivity of the composite material decreases, which limits the rapid conduction of heat from the MOSFET area to the cooling area, resulting in heat retention in some areas.

In summary, under the medium porosity (0.5–0.7), the PCM+MF structure achieves a balance between the heat conduction path and the phase change heat storage capacity, which can significantly improve the thermal management performance of the MOSFET area, reduce the temperature peak and improve the uniformity of

the temperature field, verifying the thermal optimization potential of the structure under dynamic heat load conditions.

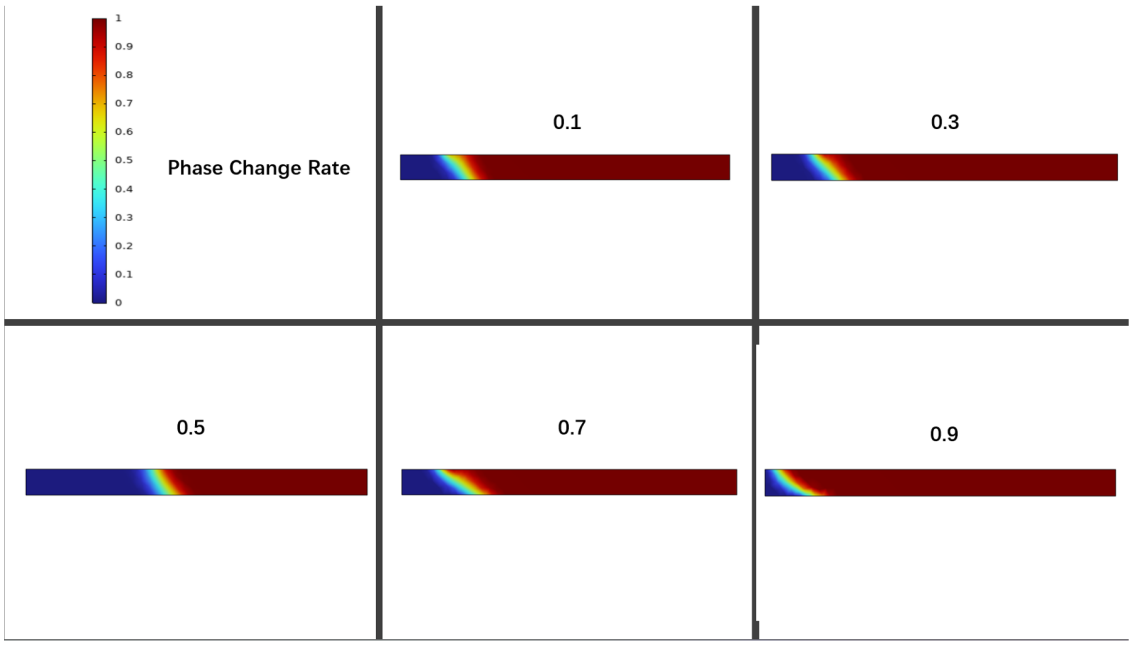

Figure 4.10: The distribution of phase change rate in the PCM region under different porosities (0.1, 0.3, 0.5, 0.7 and 0.9) at t = 100 s

Figure 4.10 shows the distribution of phase change rate in the PCM region under different porosities (0.1, 0.3, 0.5, 0.7 and 0.9) at t = 100 s, showing the melting state of the PCM+MF structure under the heat source (MOSFET) in the form of a longitudinal section.

The redder the color in the figure, the higher the phase change rate, that is, the PCM has completely melted, and the blue indicates that it is still in a solid state or partially melted. From the overall distribution trend, the phase change area is generally concentrated in the lower right. This is because the coolant flows from left to right. As the distance increases, its temperature increases and the heat transfer capacity decreases. The right area is easier to maintain high temperature, resulting in more complete melting of the PCM.

When the porosity is 0.5, although only the PCM in the right half of the figure is completely melted and the phase change degree in the left half is low, this configuration shows the lowest MOSFET temperature. This result shows that the quality of thermal management depends not only on the absolute area of the melting range, but also on the efficiency of the thermal conduction path and the heat-fluid synergy mechanism. The structure with a porosity of 0.5 achieves a good balance between the metal foam skeleton and the PCM volume distribution: its skeleton thermal conduction network is sufficient to quickly conduct heat to the bottom, while retaining enough PCM volume for absorbing heat and forming an effective coupled heat exchange interface with the coolant. This configuration achieves a high thermal

response efficiency, and can quickly reduce the heat source temperature even if the melting area is not "comprehensive".

In contrast, when the porosity is 0.1 and 0.3, the metal foam content is high and the thermal conductivity is strong, but the available PCM content is low and the heat storage capacity is insufficient, resulting in the rapid melting of the PCM but it is difficult to continue the thermal buffering effect, and there is still a high temperature area near the MOSFET; especially when the porosity is 0.1, almost the entire PCM area quickly reaches saturation and loses further heat absorption capacity.

When the porosity is 0.7 and 0.9, although the PCM content is sufficient and the latent heat capacity is large, the skeleton heat conduction network is weakened, and the heat is difficult to quickly transfer to the deep part of the PCM. In addition, the heat exchange capacity of the coolant at the right end is significantly reduced, resulting in heat retention inside the PCM, forming a large-scale continuous high-temperature melting area, but it is unable to take away the heat in time, and the MOSFET temperature eventually rises.

In summary, although the phase change area is not the largest when the porosity is 0.5, the optimal synergy is formed between its heat dissipation path, heat exchange efficiency and heat storage capacity, which is the configuration option with the best thermal control performance in this study.

4.3 A new design

The previous simulation results performed well overall, but there is still room for optimization. We still haven't seen the temperature remain constant, and the temperature on the MOSFET is still changing, which may cause greater thermal stress and accelerate its aging. Therefore, the existing design still needs to be further optimized, and the focus should be on slowing down its temperature rise rate to achieve better thermal management performance and longer device life.

4.3.1 The effect of the cylindrical structure

Combined with the above simulation results, it can be seen that although the overall thermal conductivity is improved by introducing the equivalent thermal conductivity of the metal foam enhanced phase change material (PCM) region, there are still certain limitations in the transfer of heat from the heat source to the direction away from the heat source, resulting in uneven temperature field distribution inside the PCM. To be more specific, the PCM on the side close to the heat source melts first, while the area away from the heat source remains in solid state and fails to fully participate in the heat absorption process. This uneven heat distribution limits the utilisation efficiency of the PCM, thus affecting the overall thermal management effect. In order to further improve the coverage of the heat conduction path, this paper introduces a copper cylinder as a high thermal conductivity heat extension element based on the metal foam structure to enhance the ability to transfer heat to

the area far from the heat source, thereby achieving a more balanced temperature distribution. The structural design is shown in the figure 4.11.

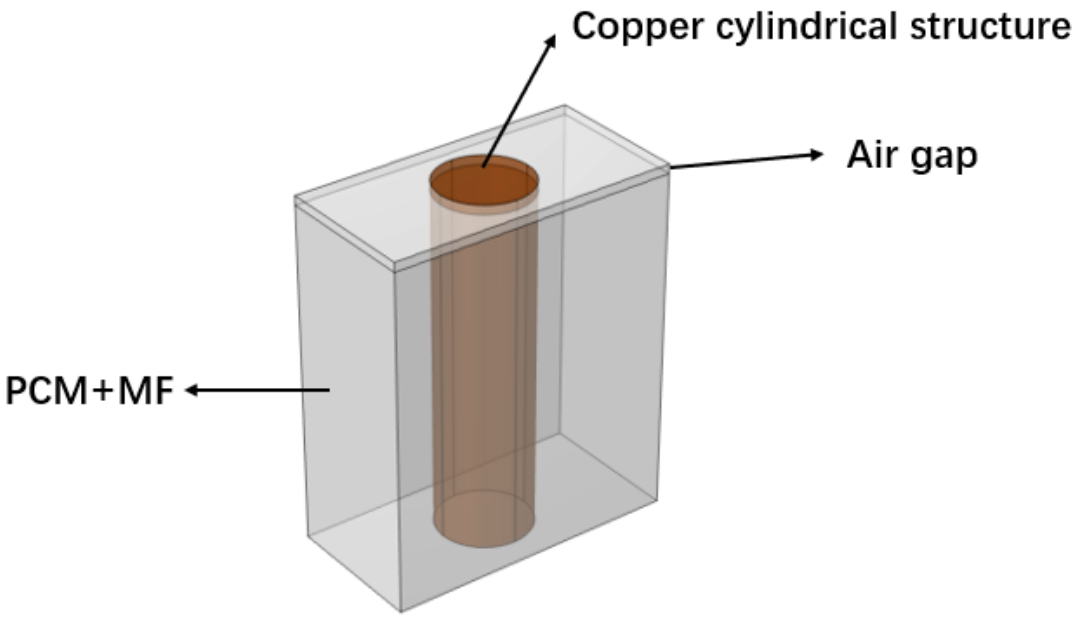

Figure 4.11: Cylindrical structure

This model can be regarded as a local substructure in the previous PCM+MF composite structure model, and its geometric configuration and material parameters are consistent. In order to ensure the comparability and continuity between the simulation results, this study uses the heat flux distribution obtained in the previous model as the boundary heat input condition of this model, so that the transient temperature response characteristics of the structure can be analyzed under a unified heat load background.

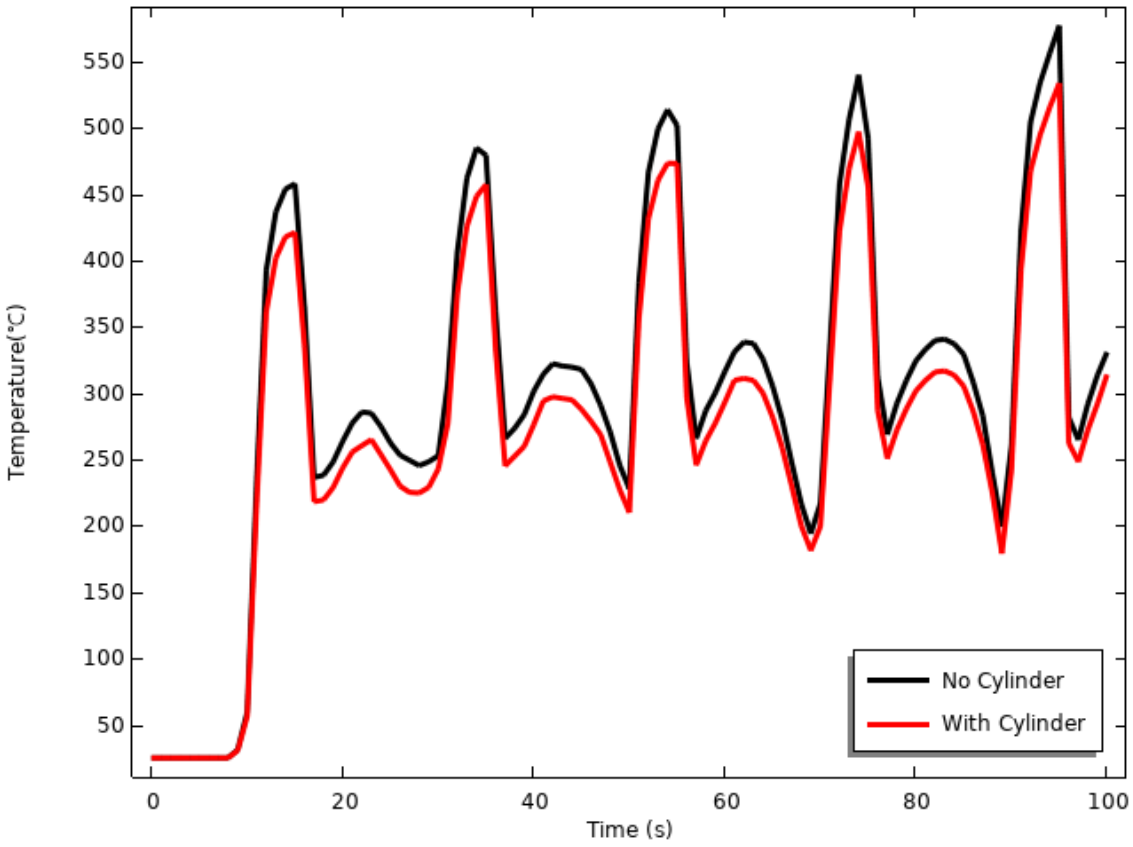

Figure 4.12: Comparison of temperature response with and without copper cylindrical structure

Figure 4.12 shows the temperature change of the heat source area in the first 100 seconds under two working conditions with and without the copper cylindrical structure. It can be observed that under the same porosity conditions, the introduction of the cylindrical structure significantly reduces the temperature peak at the heat source, reflecting a better initial stage thermal control effect.

4.3.2 Integrating cylindrical structures into realistic models

After verifying the effectiveness of the copper cylindrical structure in promoting heat diffusion, this paper further integrates the structure into the radiator system. In order to enhance the modularity of the thermal management structure and provide clearer thermal response analysis conditions for subsequent research, copper partition walls are introduced in the physical structure to divide the PCM area into multiple independent units. This structural design helps control the local heat flow path, enhances the controllability of the system's thermal response, and lays the foundation for comparative analysis of the heat transfer characteristics of different units.

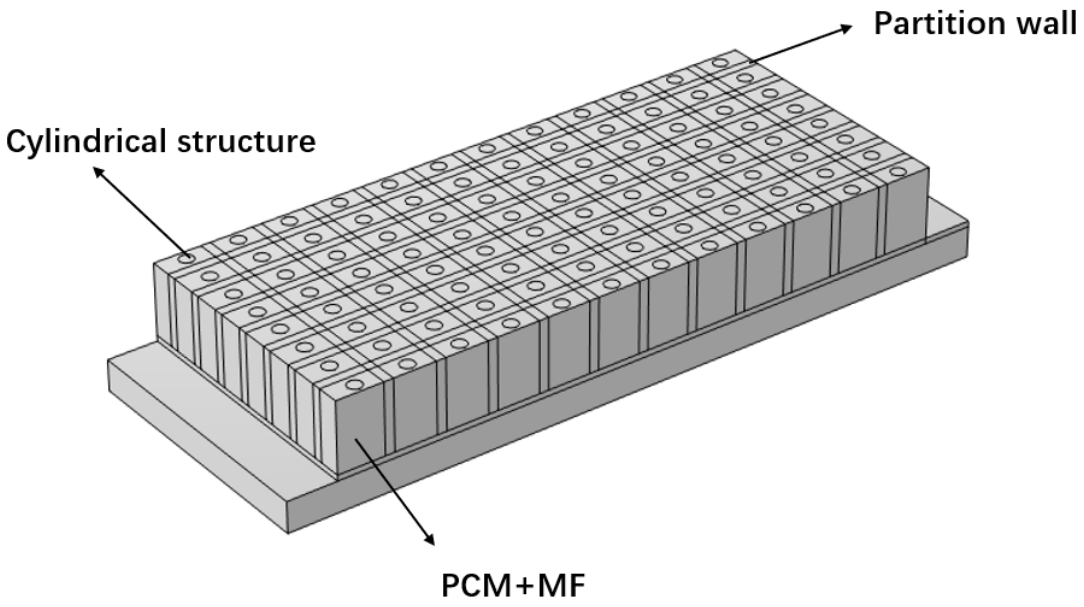

Figure 4.13: Integrated cylindrical heat sink

Figure 4.13 illustrates the modified heat sink model with the integrated copper pillar structure. The structure introduces longitudinal copper columns as a high thermal conductivity path through which heat can be transferred more quickly to the bottom position of the heat sink. To ensure the comparability of the results, after the model is built, the same boundary conditions (including heat flux, ambient temperature, and convection heat transfer coefficient, etc.) as the aforementioned copper-free structure model are used for simulation calculations to ensure the attributability of thermal response differences between different structures.

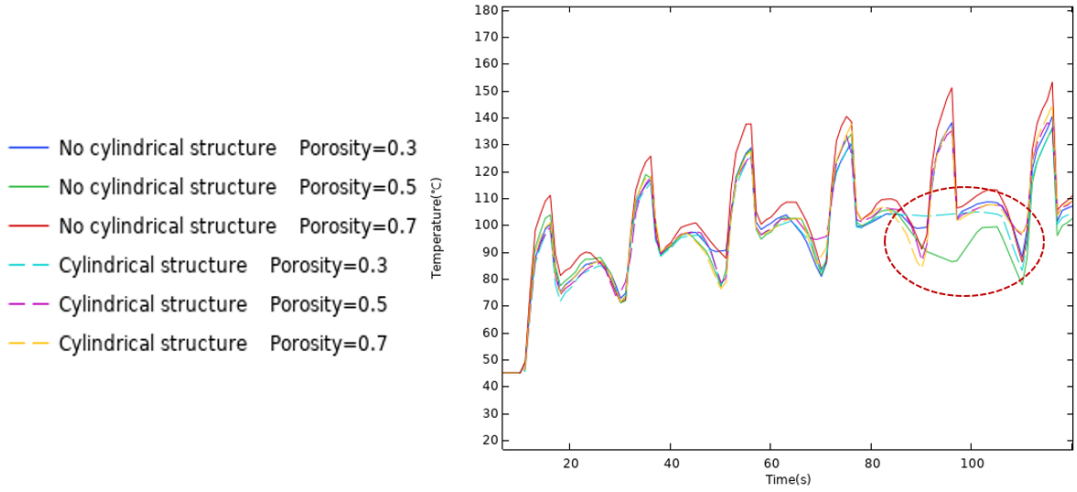

Figure 4.14: Comparison of temperature response of MOSFET devices with and without copper cylindrical structures at different porosity conditions

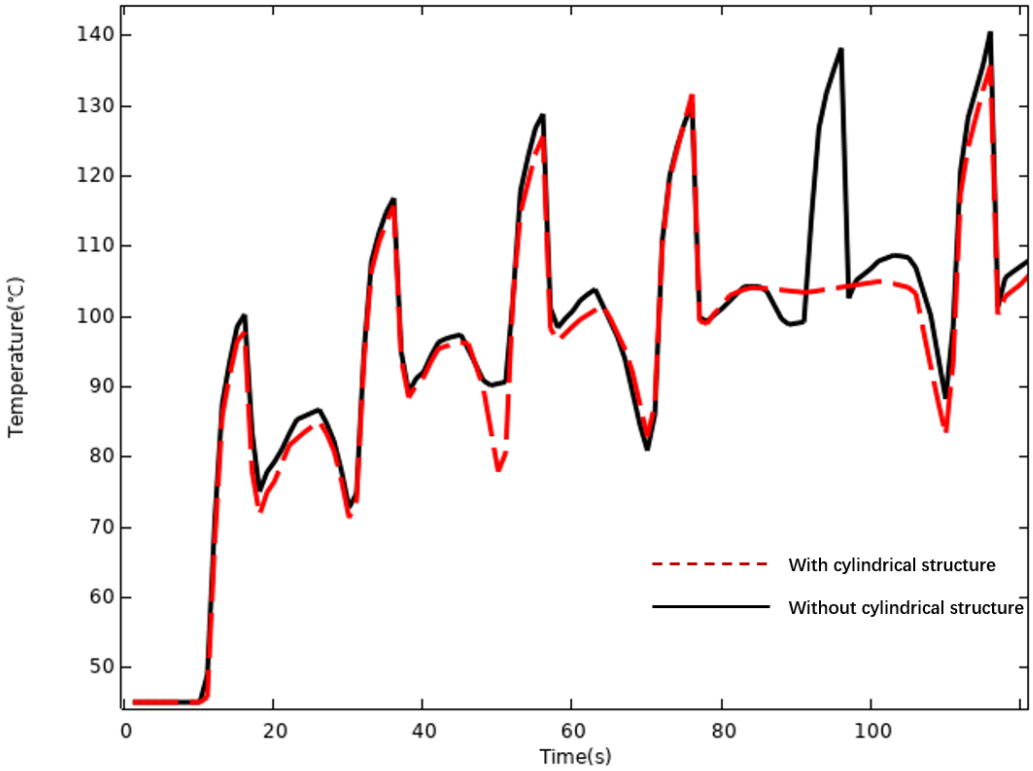

Figure 4.15: Temperature variation on MOSFET with and without cylindrical structure at porosity 0.3

It can be observed from Figure 4.14 that the introduction of the copper cylindrical structure under different porosity conditions has a positive effect on the temperature

control of the MOSFET device. Compared with the structure without the introduction of the copper column, after adding the high thermal conductivity channel, the surface temperature of the MOSFET has decreased to a certain extent at each porosity level, reflecting the universality and effectiveness of the structure in improving the thermal diffusion efficiency.

In addition, it is worth noting that when the porosity is 0.3, the system thermal management performance shows significant advantages. Specifically, in the fifth driving cycle stage, the temperature of the MOSFET device remained basically stable, maintained at about 103°C, and lasted for about 25 seconds, indicating that the system can effectively suppress the rapid rise and fluctuation of the device temperature under this configuration. This long-term thermal stability can reduce thermal stresses, slow material aging, and improve device operational reliability.

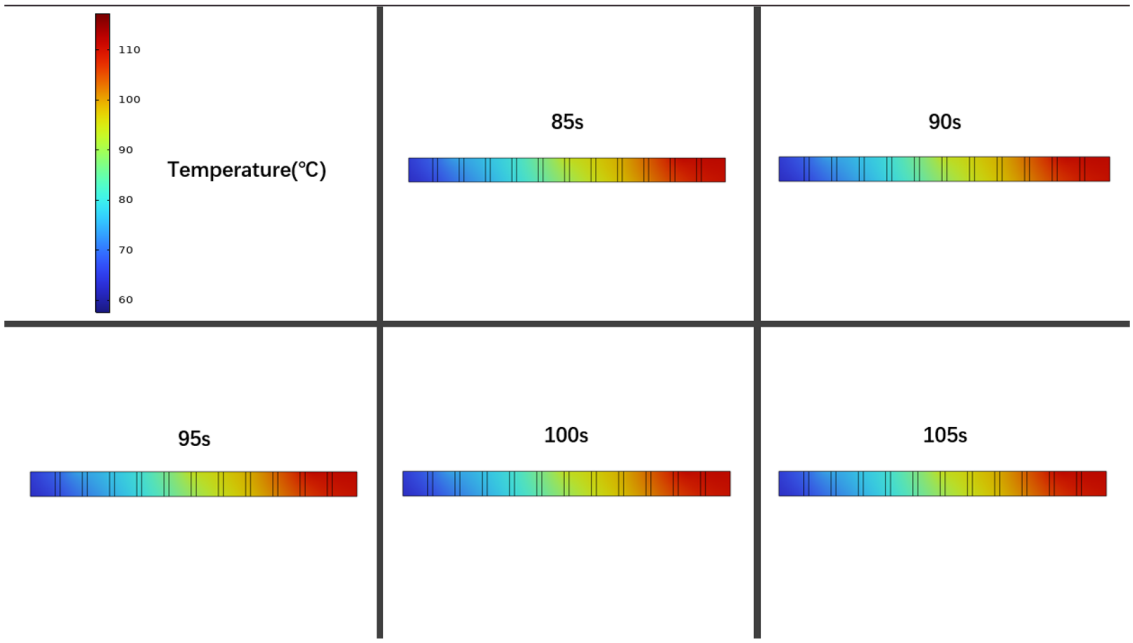

Figure 4.16: Temperature distribution of PCM area at each time in the fifth cycle when there is a cylindrical structure

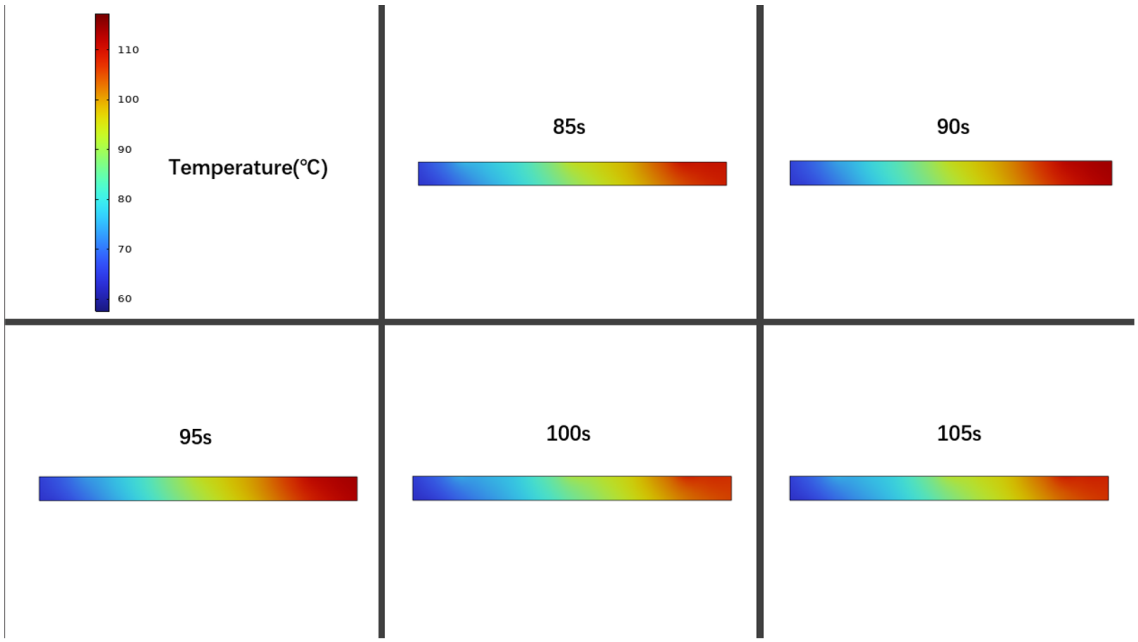

Figure 4.17: Temperature distribution of PCM area at each moment in the fifth cycle without cylindrical structure

In order to compare the thermal management behaviors of different structures in the fifth driving cycle, Figures 4.16 and 4.17 show the cross-sectional temperature distribution of the PCM region at 85 s, 90 s, 95 s, 100 s and 105 s respectively when the porosity is 0.3 and 0.5 with and without the addition of the copper cylindrical structure. It should be pointed out that in this model, the coolant continues to flow, and its flow direction has a certain intersection with the heat transfer path of the PCM region under the heat source. Therefore, the temperature field inside the PCM is affected by both fluid cooling and local thermal conductivity, especially the inhomogeneity of temperature distribution in the flow direction is more obvious.

It can be observed from Figure 4.16 that under the condition of introducing the copper column structure, although the coolant continues to take away heat, the entire PCM region still maintains a relatively stable temperature field distribution during the above time period. In particular, in the direction of coolant flow, the temperature gradient is significantly suppressed, showing stronger heat diffusion ability and uniformity. Correspondingly, the temperature of the MOSFET device is maintained at about 103℃ for more than 25 seconds, indicating that the system has formed a relatively stable thermal equilibrium in this state. This shows that the copper pillar not only enhances the radial heat diffusion capacity of the PCM area, but also improves the uniformity of temperature distribution along the flow direction, thereby suppressing local heat accumulation and temperature fluctuations.

In contrast, the temperature distribution under the copper pillar-free structure shown in Figure 4.17 shows certain dynamic change characteristics. Although the temperature of the MOSFET has been significantly improved compared with the original unfilled PCM structure, its temperature still shows a continuous change

trend, and the temperature distribution inside the PCM is uneven, especially in the direction of coolant flow. The temperature of the area close to the heat source or the coolant outlet rises rapidly and completes the phase change in advance, while the area far away from the heat source and close to the initial inlet direction of the coolant remains in a low-temperature solid state, indicating that the heat transfer speed in the PCM is limited and the thermal capacity advantage of the entire phase change material cannot be mobilized in time.

In summary, the addition of the copper pillar structure not only improves the thermal conductivity near the heat source, but also optimizes the thermal uniformity of the PCM area in the direction of coolant flow, significantly prolonging the MOSFET temperature plateau period, reflecting its effectiveness in regulating the local heat conduction path in a complex cooling environment. This result further demonstrates the considerable potential of the structure we used to improve the thermal management performance of electronic devices.

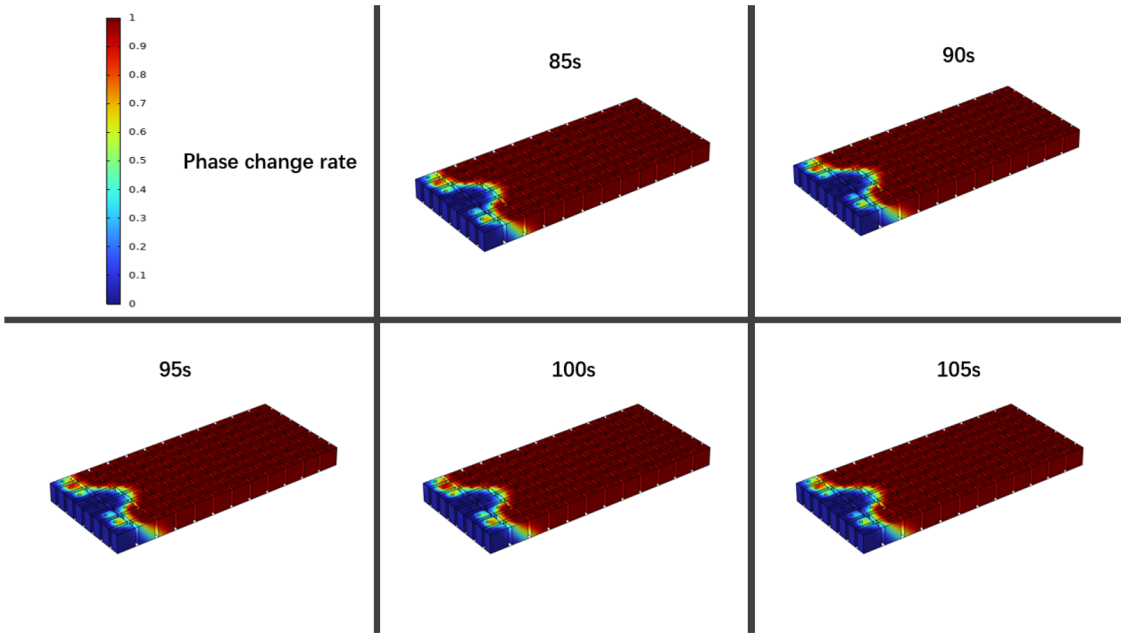

Figure 4.18: Phase change rate diagram of PCM region of integrated copper pillar structure at different time points (85s, 90s, 95s, 100s, 105s)

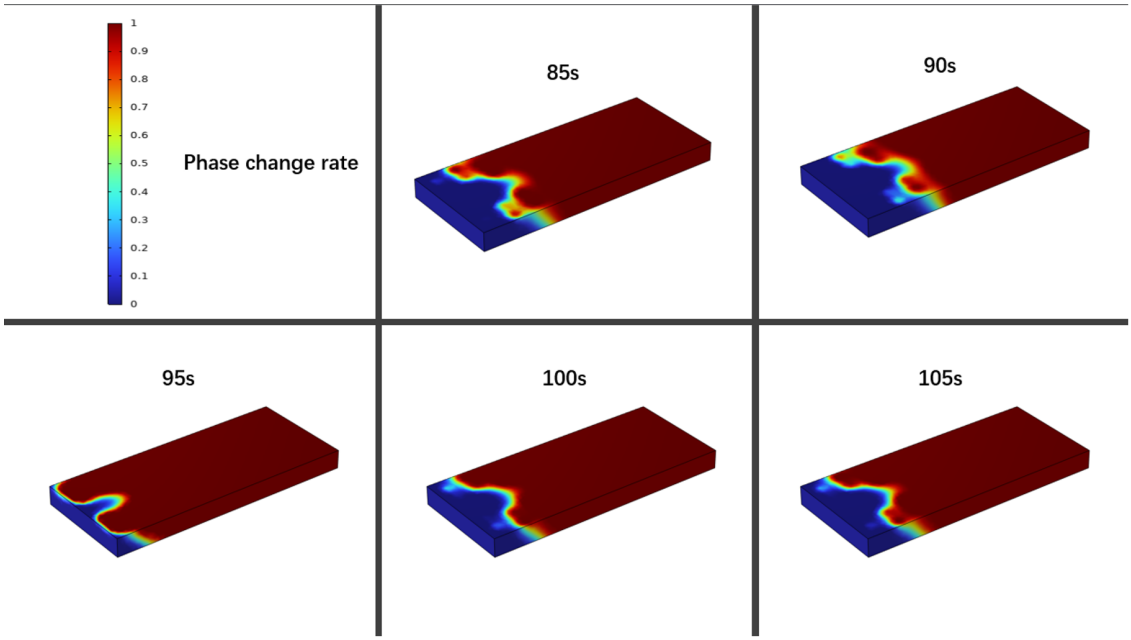

Figure 4.19: Phase change rate diagram of PCM region without copper pillar structure at different time points (85s, 90s, 95s, 100s, 105s)

After the copper pillar structure was introduced, an obvious temperature platform period was also formed inside the PCM region.Temperature platform refers to the phenomenon that the temperature of a material remains approximately constant while continuously absorbing heat over a period of time. When the copper pillar structure was not set, the PCM phase change process was significantly delayed. The appearance of the temperature platform indicates that the system has entered a thermal equilibrium stage dominated by latent heat absorption, that is, the heat continuously input by the heat source is mainly used to drive the phase change, and the temperature remains constant temporarily, which is consistent with the thermodynamic characteristics of the typical PCM phase change process.

Upon further examination of the results we found that the melting in the PCM region is higher when a copper column structure is present, especially in the region away from the coolant inlet, where the PCM undergoes essentially a complete phase transition. While when there is no copper pillar structure, there is still a large unmelted area in the same period, and the change over time is more dramatic, reflecting the unevenness of the system in thermal distribution. In particular, the PCM close to the coolant inlet is subject to the strong cooling effect of the coolant, and is prone to local overcooling or incomplete phase change in multiple cycles, resulting in some areas remaining in liquid or solid at the end of the cycle, with the initial state of "uncompleted phase change" remaining. Experimental studies at universities such as Purdue University have verified this cyclic residual effect: if the PCM is not fully solidified at the end of a cycle, the latent heat available to the PCM is reduced during the following warming process, a phenomenon that affects the thermal management efficiency of the system (Ieee.org, 2024).

In addition, the introduction of copper pillars and copper isolation walls significantly improves the thermal conductivity of PCM. Literature points out that high thermal conductivity structures such as copper pillars or metal foams can form a heat conduction network in PCM, which can improve the overall heat transfer efficiency and temperature uniformity by shortening the heat diffusion path, enhancing liquid phase natural convection, and balancing heat capacity distribution (Buonomo et al., 2022). Our results also confirm their theory that the PCM far away from the coolant inlet region can also effectively complete the phase transition after the addition of the copper column structure, showing that the heat can be more uniformly distributed throughout the phase transition region, avoiding localised overheating or unmelting.

In summary, the temperature platform phenomenon observed in this study is consistent with existing thermodynamic theories and experimental results (Maxa, Novikov and Nowottnick, 2017), reflecting the physical mechanism of temporary balance between latent heat absorption and heat input; at the same time, under the actual working conditions of flow cooling and multiple cycles, local supercooling, incomplete phase change and thermal residue objectively exist, and the copper column structure effectively alleviates these problems by optimizing the heat diffusion path, improving the thermal response consistency and reliability of the system. The above analysis verifies the importance of structural design in the composite PCM thermal management system, and also provides a theoretical basis and engineering reference for subsequent optimization.

4.3.3 Optimization

It is worth noting that in the aforementioned structural optimization scheme, we have achieved some remarkable results. For example, in the 5th driving cycle, we noticed that the system temperature seemed to be nearly constant. However, in practical applications, electronic modules are more susceptible to instantaneous temperature rise in the initial heating stage. Therefore, another goal of the optimization in this section is to further reduce its temperature change rate for the first driving cycle and delay the arrival of the peak temperature, thereby improving the initial thermal buffering capacity and system safety.

Firstly, since the content of PCM will have an impact on the results of thermal management, we are going to adjust the thickness of the PCM area to change the total amount of PCM..Secondly, considering that the cylindrical structure played a positive role in promoting phase change in the distal region in the previous results, we tried to optimize the radius of the cylinder to further improve the heat transfer efficiency. Changes in the size of the cylinder will directly affect the coverage of its thermal network and the ability to guide heat flow, which may play an important role in balancing heat distribution.

In addition, inspired by references Kotb and Wang (2024) and Bian et al(2024), we introduced a nonlinear gradient porosity structure to explore its performance improvement potential under the condition of coolant flow. Previous studies have

shown that foam structures along different porosities can significantly improve the heat transfer efficiency and phase change uniformity of PCM. Therefore, combined with the characteristics of continuous flow of coolant in one direction in this model, we try to introduce a gradient porous structure in the PCM region, that is, the PCM region is divided into three sub-regions according to the coolant flow direction, and different porosities are set for each sub-region to achieve segmented optimization and local thermal regulation. This zoning design also takes into account the heat source distribution of the three power modules at the top of the radiator, further improving heat transfer coordination through space matching.

In summary, this section will propose and verify a series of optimization schemes from multiple dimensions such as geometric structure, material distribution and heat source coupling to further enhance the thermal management performance of the PCM-coolant coupling system.

4.3.3.1 Parameters

As mentioned above, this study selected five key structural parameters as optimization variables, namely the thickness Th of the PCM region, the radius r of the copper cylindrical structure, and the porosity parameters por_1, por_2 and por_3 of the three sub-regions divided along the coolant flow direction.
These parameters were selected to study the effect of porosity distribution, copper cylinder size and PCM content on the overall thermal management effect, and the specific range of values for each parameter is shown in the table 4.1. Figure 4.20 illustrates the spatial distribution of different porosity regions in the porous structure in the geometric model, where Region 1, Region 2 and Region 3 correspond to the upstream, midstream and downstream positions on the coolant flow path, respectively, to achieve gradient structure optimization design that conforms to the flow direction.

Parameter name	Range	Unit	Description
Th	0.01-0.02	m	Thickness of PCM area
r	0.001-0.002	m	Cylinder radius
Por1	0.1-0.9	-	Porosity of region 1
Por2	0.1-0.9	-	Porosity of region 2
Por3	0.1-0.9	-	Porosity of region 2

Table 4.1: Optimization parameters and their value ranges

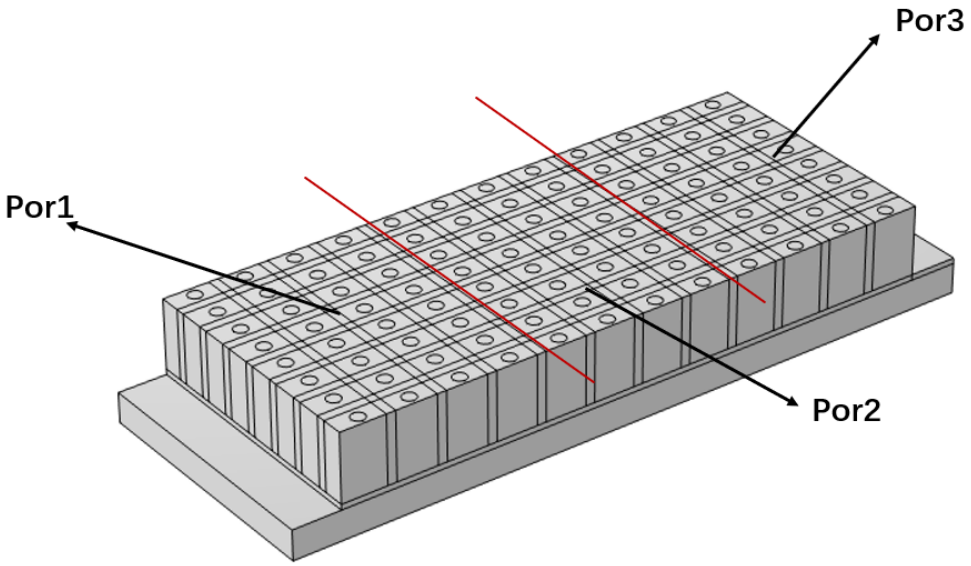

Figure 4.20: Schematic diagram of spatial distribution of regions with different porosity

4.3.3.2 Optimization methods and goal setting

Our objective is to reduce the rate of change of the surface temperature of the MOSFET during the first heating cycle (0 to 30 seconds) in order to reduce the risk of thermal shock to the MOSFET. To quantify this objective, the following objective function is defined:

$$\min \left(\int_0^{30} \left| \frac{d\, T_{\mathrm{MOSFET}}(t)}{dt} \right| dt \right) \tag{4.1}$$

Among them, $T_{\mathrm{MOSFET}}(t)$represents the average temperature of the MOSFET surface at time t, the absolute value operation ensures that the total thermal shock caused by the temperature rise and fall is considered, and the time integral is used to measure the total temperature fluctuation intensity within the entire first cycle. This definition not only helps to keep the objective function in a low dimension, but also effectively reduces the computational burden in the model optimization process.

In order to minimise the above objectives, this paper adopts the Boundary Optimisation Quadratic Approximation (BOBYQA) algorithm for optimisation.BOBYQA is an iterative optimisation method based on the domain of reliance, which is suitable for solving the optimisation problems of continuous variables, and is especially suitable for the complex multi-physics field models where the objective function is non-differentiable or difficult to discretise. It shows good stability and convergence speed. Since the thermal simulation model in this study is a nonlinear, strongly coupled transient heat transfer problem, the derivative of the objective function is difficult to obtain explicitly, so the use of BOBYQA can effectively avoid dependence on gradient information and reduce the risk of numerical instability.

In the optimisation process, the convergence tolerance is set to 0.001 and the maximum number of iterations is limited to 2000

4.3.3.3 Optimization results

Table 4.2 shows the best parameters obtained. Under this parameter combination, the temperature change of the mosfet in the first cycle is the smallest.

Parameter name	Th	r	Por1	Por2	Por3
Value	0.015	0.0015	0.58	0.6	0.8

Table 4.2: Optimal parameters

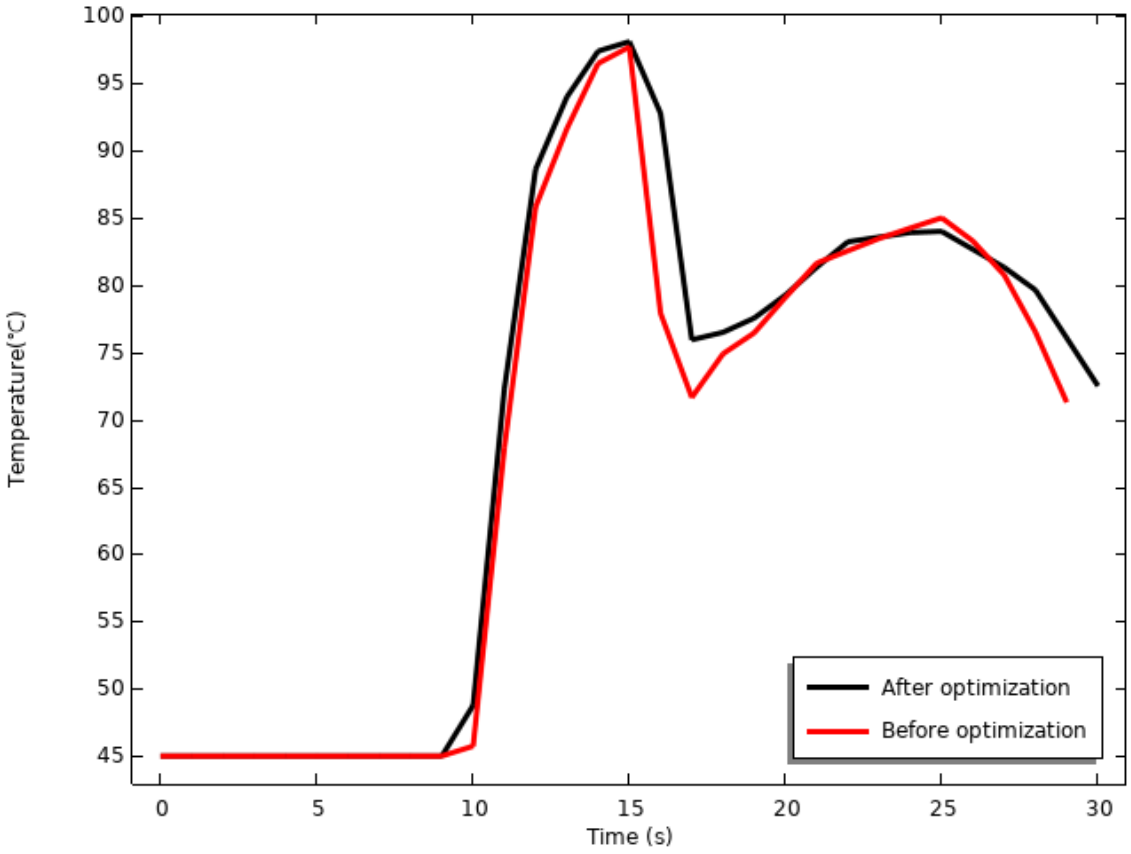

Figure 4.21: Comparison of MOSFET Temperature Variation in the First Driving Cycle Before and After Optimization

Figure 4.21 shows the comparison of the temperature change of the MOSFET chip area in the first driving cycle before and after optimization. It can be clearly observed from the figure that after the structural parameter optimization, the temperature change rate of the MOSFET has been significantly reduced throughout the cycle.

Specifically, in the deceleration stage before optimization (about 17-30 s period), the average temperature of the MOSFET rose by about 13°C in 8 seconds, showing

an obvious temperature rise jump phenomenon. After multi-parameter joint optimization (including phase change material area thickness, copper column radius and porosity partitioning), the temperature in the same time period only rose by about 8°C, and the temperature change rate was reduced by nearly 40% compared with the original structure, indicating that the optimization significantly alleviated the thermal shock effect in the initial stage.
In addition, from the perspective of temperature peak, the optimization scheme significantly reduced the temperature change rate without bringing additional peak temperature rise. The maximum temperature of the two schemes is basically the same, indicating that the optimization strategy maintains the overall thermal stability of the system while improving the thermal buffering capacity. The results further validate that this improved structure improves thermal management performance, especially in the most critical first cycle, successfully controlling the thermal response rate and reducing the thermal shock suffered by the MOSFETs, which helps to prolong the lifetime of the power device.

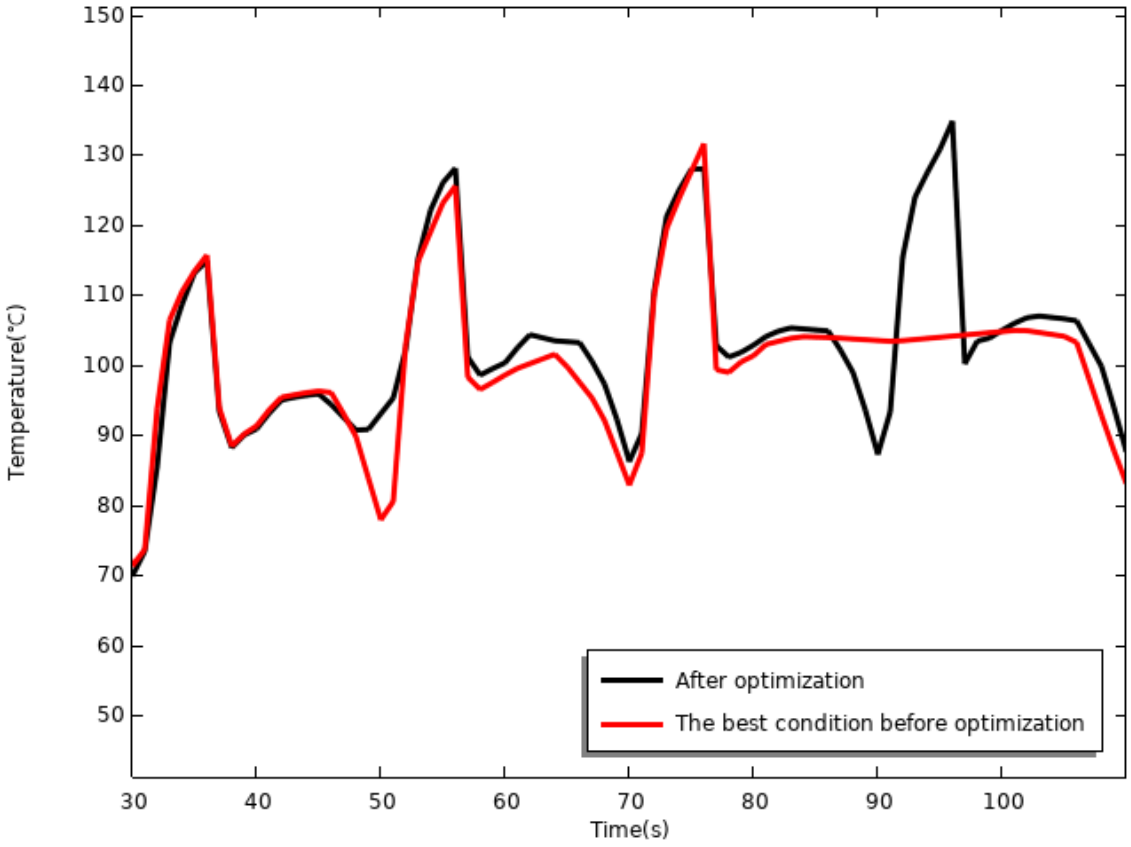

Figure 4.22: Comparison of MOSFET temperature changes from the second to the fifth cycle before and after optimization

Figure 4.22 shows the comparison curves of the temperature change of the MOSFET area over time in the second to fifth driving cycles, which correspond to the optimal operating state before structural optimization and the improved scheme after the implementation of multi-parameter structural optimization.

As can be seen from the figure, although the two groups of working conditions are consistent in the overall temperature evolution trend, the optimized results show better performance in thermal response characteristics in multiple key time periods, especially in the stage of rapid power change. Taking the second to fourth cycles as an example, the temperature change rate of the optimized scheme is significantly lower than that of the situation before optimization. For example, in the cooling section of the second cycle (about 46–52s) and the subsequent heating section of the third cycle (about 60–70s), the temperature rise and cooling rates after optimization are effectively suppressed, indicating that the transient regulation ability of the thermal management structure is enhanced.

However, it should be pointed out that although the optimization scheme effectively reduces the temperature change rate of the first four cycles and improves the stability of thermal regulation, the temperature platform that appeared in the curve before optimization, that is, the phenomenon that the temperature tends to be constant for a period of time, is not reproduced in the fifth cycle stage. This may be related to the redistribution of heat capacity distribution and phase change rate by the optimization strategy, indicating the regulatory balance limit of thermal hysteresis at a specific cycle stage.

In summary, the multi-parameter structural optimization scheme proposed in this study significantly reduces the temperature change rate of the MOSFET area within the first driving cycle, showing a certain transient thermal management capability. This makes the optimized structure have stronger thermal relief and temperature rise suppression performance under short-term operation or low-frequency conditions. For example, in urban traffic or frequent start-stop conditions, such as buses, taxis or electric delivery vehicles, the operating cycle is short and the thermal shock is frequent. The optimization scheme can effectively reduce local temperature variations, thus extending the service life of power devices and improving system safety.

However, from the temperature evolution trend, the optimization scheme did not maintain the temperature platform effect that appeared in the pre-optimization scheme. This may be because the optimized structure sacrificed part of the steady-state heat capacity while improving the response speed, resulting in the inability to maintain thermal balance for a long time in the subsequent heat accumulation stage. Therefore, the original design is more suitable in applications with continuous high load operation, as it shows constant temperature behavior in the fifth cycle, which helps to maintain the thermal stability of the system.

Therefore, the structures before and after optimization are complementary under different operating conditions: the optimized scheme is more suitable for the working mode with short thermal shock and high frequency, while the design before optimization is suitable for the steady-state scenario with high load and long operation. This finding provides a basis for the customized design of the subsequent thermal management strategy, and also suggests that in practical applications, the thermal management structure configuration should be reasonably selected according to the

vehicle usage mode.

5

Conclusion

In this study, a systematic thermal management optimisation of a battery electric vehicle (BEV) power inverter is investigated with a focus on improving its transient thermal response. The inverter structure designed in this paper integrates phase change materials (PCMs) and also uses metal foam to exploit the latent heat storage properties of the materials.

Firstly, this paper constructs a detailed thermal model of the inverter in Comsol and establishes a thermal input model that can dynamically calculate the switching loss and conduction loss of the MOSFET device according to the actual driving conditions in Matlab, which provides a reliable basis for analysing its transient temperature rise behaviour.

Immediately following this, we explored the combined PCM+MF structure and showed that the system exhibits a significant temperature drop and an approximate temperature constancy in the 5th drive cycle when the porosity is 0.3. Then, a composite structure of a copper cylinder with an insulating wall was introduced, and the results showed that a constant temperature occurred at a porosity of 0.5. This shows that this structure further improves the buffering capacity of the system against repetitive heat input.

Through parameter sensitivity analysis, it is found that the thickness of the PCM area, the radius of the embedded copper pillars, and the spatial distribution porosity of the metal foam all significantly affect the transient heat transfer process. Drawing on the research results of previous researchers, this paper adopts a porous layout with nonlinear gradient changes in the coolant flow direction, thereby improving the local heat dissipation performance without increasing the peak temperature.

In order to further improve the thermal response performance of the system, the BOBYQA algorithm is used for multi-parameter joint structural optimization. The optimization goal is set to minimize the average temperature change rate of the MOSFET in the first round of driving cycles, aiming to minimize the cumulative effect of initial thermal shock and device fatigue. The simulation results verify the effectiveness of the optimization scheme in reducing the temperature gradient, while not causing an increase in the peak temperature of the device.

Comparative analysis shows that the optimized structure significantly suppresses the temperature rise rate in the acceleration and deceleration stages of the first few

driving cycles, and is more suitable for urban traffic scenarios with frequent start-stop or short-term load surges. The structure before optimization has a stronger thermal inertia, and the temperature tends to be stable in subsequent cycles, which is more suitable for steady-state conditions with long continuous loads and slow heat input, such as high-speed cruising or long-distance transportation.

In summary, by introducing phase change materials, metal foams and copper reinforcement structures, combined with reasonable structural partitioning and multi-parameter optimization strategies, Thermal management of power inverters can be improved by approximately 40%, and its peak temperature and temperature change rate can be reduced, thereby effectively alleviating thermal shock, extending the service life of the device, and providing a feasible solution for the design of the next-generation power electronic system for electric transportation.

Bibliography

[1] Jaramillo, P., Kahn, S., Ribeiro, P., Newman, S., Dhar, O., Diemuodeke, T., Kajino, D., Lee, S., Nugroho, X., Ou, A., Hammer, S., Shukla, J., Skea, R., Slade, A., Al Khourdajie, R., Van Diemen, D., Mccollum, M., Pathak, S., Some, P. and Vyas, R. (2022). Simon Robertson (Australia), Andrea Santos (Brazil), Karen C. Seto (the United States of America). Rohit Sharma. [online] doi:https://doi.org/10.1017/9781009157926.012.

[2] Cambridge University Press. (n.d.). Summary for Policymakers. [online] Available at: https://www.cambridge.org/core/books/climate-change-2022-mitigation-of-climate-change/summary-for-policymakers/ABC31CEA863CB6AD8FEB6911A872B321.

[3] Jaguemont, J., Boulon, L. and Dubé, Y. (2016). A comprehensive review of lithium-ion batteries used in hybrid and electric vehicles at cold temperatures. Applied Energy, 164, pp.99–114. doi:https://doi.org/10.1016/j.apenergy.2015.11.034.

[4] Zhang, Y., Liu, X., Wei, W., Peng, T., Hong, G. and Meng, C. (2020). Mobile charging: A novel charging system for electric vehicles in urban areas. Applied Energy, 278, p.115648. doi:https://doi.org/10.1016/j.apenergy.2020.115648.

[5] Wang, W., Niu, J., Li, Y. and Ren, K. (2022). Numerical study on heat transfer enhancement by spray-sublimation cooling with dry ice particles. Applied Thermal Engineering, [online] 214, p.118809. doi:https://doi.org/10.1016/j.applthermaleng.2022.118809.

[6] Erp, R. van, Georgios Kampitsis and Elison Matioli (2019). Efficient Microchannel Cooling of Multiple Power Devices With Compact Flow Distribution for High Power-Density Converters. IEEE Transactions on Power Electronics, 35(7), pp.7235–7245. doi:https://doi.org/10.1109/tpel.2019.2959736.

[7] Cai, Y., Liu, D., Zhao, F.-Y. and Tang, J.-F. (2016). Performance analysis and assessment of thermoelectric micro cooler for electronic devices. Energy Conversion and Management, 124, pp.203–211. doi:https://doi.org/10.1016/j.enconman.2016.07.011.

[8] Lajunen, A., Yang, Y. and Emadi, A. (2018). Recent Developments in Thermal Management of Electrified Powertrains. IEEE Transactions on Vehicular Technology, 67(12), pp.11486–11499. doi:https://doi.org/10.1109/tvt.2018.2876315.

[9] Wang, X., Li, B., Gerada, D., Huang, K., Stone, I., Worrall, S. and Yan, Y. (2022b). A critical review on thermal management technologies for motors in electric cars. Applied Thermal Engineering, 201, p.117758. doi:https://doi.org/10.1016/j.applthermaleng.2021.117758.

[10] Lei, S., Xin, S. and Liu, S. (2022). Separate and integrated thermal management solutions for electric vehicles: A review. Journal of Power Sources, 550, pp.232133–232133. doi:https://doi.org/10.1016/j.jpowsour.2022.232133.

[11] Gautier Rouaze, Marcinichen, J.B., Cataldo, F., Aubin, P. and Thome, J.R. (2021). Simulation and experimental validation of pulsating heat pipes. Applied Thermal Engineering, 196, pp.117271–117271. doi:https://doi.org/10.1016/j.applthermaleng.2021.117271.Lei, S., Xin, S. and Liu, S. (2022). Separate and integrated thermal management solutions for electric vehicles: A review. Journal of Power Sources, 550, pp.232133–232133. doi:https://doi.org/10.1016/j.jpowsour.2022.232133.Wang, X., Li, B., Gerada, D., Huang, K., Stone, I., Worrall, S. and Yan, Y. (2022b). A critical review on thermal management technologies for motors in electric cars. Applied Thermal Engineering, 201, p.117758. doi:https://doi.org/10.1016/j.applthermaleng.2021.117758.

[12] Chang, T.-C., Lee, S., Fuh, Y.-K., Peng, Y.-C. and Lin, Z.-Y. (2017). PCM based heat sinks of paraffin/nanoplatelet graphite composite for thermal management of IGBT. Applied Thermal Engineering, 112, pp.1129–1136. doi:https://doi.org/10.1016/j.applthermaleng.2016.11.010.

[13] Han, F., Guo, H. and Ding, X. (2021). Design and optimization of a liquid cooled heat sink for a motor inverter in electric vehicles. Applied Energy, 291, p.116819. doi:https://doi.org/10.1016/j.apenergy.2021.116819.

[14] Huseyin Bostanci, Ee, D.V., Saarloos, B.A., Rini, D.P. and Chow, L.C. (2012). Thermal Management of Power Inverter Modules at High Fluxes via Two-Phase Spray Cooling. IEEE Transactions on Components Packaging and Manufacturing Technology, 2(9), pp.1480–1485. doi:https://doi.org/10.1109/tcpmt.2012.2190933.

[15] Wang, P., McCluskey, P. and Bar-Cohen, A. (2013). Two-Phase Liquid Cooling for Thermal Management of IGBT Power Electronic Module. Journal of Electronic Packaging, 135(2). doi:https://doi.org/10.1115/1.4023215.

[16] Mehwish Mahek Khan, Alkhedher, M., Ramadan, M. and Ghazal, M. (2023). Hybrid PCM-based thermal management for lithium-ion batteries: Trends and challenges. Journal of energy storage (Print), 73, pp.108775–108775. doi:https://doi.org/10.1016/j.est.2023.108775.

[17] İsmail Gürkan Demirkıran, Oliveira, A. and Erdal Cetkin (2022). Emergence of asymmetric straight and branched fins in horizontally oriented latent heat thermal energy storage units. International Journal of Heat and Mass Transfer/International journal of heat and mass transfer, 189, pp.122726–122726. doi:https://doi.org/10.1016/j.ijheatmasstransfer.2022.122726.

[18] Gil, A., Medrano, M., Martorell, I., Lázaro, A., Dolado, P., Zalba, B. and Cabeza, L.F. (2010). State of the art on high temperature thermal energy storage for power generation. Part 1—Concepts, materials and modellization. Renewable and Sustainable Energy Reviews, [online] 14(1), pp.31–55. doi:https://doi.org/10.1016/j.rser.2009.07.035.

[19] Al-Salami, H.A., Dhaidan, N.S., Abbas, H.H., Al-Mousawi, F.N. and Homod, R.Z. (2024). Review of PCM charging in latent heat thermal energy

storage systems with fins. Thermal Science and Engineering Progress, 51, pp.102640–102640. doi:https://doi.org/10.1016/j.tsep.2024.102640.

[20] Low, Z.H., Qin, Z. and Duan, F. (2024). A review of fin application for latent heat thermal energy storage enhancement. Journal of Energy Storage, 85, p.111157. doi:https://doi.org/10.1016/j.est.2024.111157.

[21] Cui, W., Si, T., Li, X., Li, X., Lu, L., Ma, T. and Wang, Q. (2022). Heat transfer enhancement of phase change materials embedded with metal foam for thermal energy storage: A review. Renewable & Sustainable Energy Reviews, 169, pp.112912–112912. doi:https://doi.org/10.1016/j.rser.2022.112912.

[22] Shi, J., Du, H., Chen, Z. and Lei, S. (2023). Review of phase change heat transfer enhancement by metal foam. Applied Thermal Engineering, 219, pp.119427–119427. doi:https://doi.org/10.1016/j.applthermaleng.2022.119427.

[23] Sharma, A., Tyagi, V.V., Chen, C.R. and Buddhi, D. (2009). Review on thermal energy storage with phase change materials and applications. Renewable and Sustainable Energy Reviews, 13(2), pp.318–345. doi:https://doi.org/10.1016/j.rser.2007.10.005.

[24] Abhat, A. (1983). Low temperature latent heat thermal energy storage: Heat storage materials. Solar Energy, 30(4), pp.313–332. doi:https://doi.org/10.1016/0038-092x(83)90186-x.

[25] Hasnain, S.M. (1998). Review on sustainable thermal energy storage technologies, Part I: heat storage materials and techniques. Energy Conversion and Management, [online] 39(11), pp.1127–1138. doi:https://doi.org/10.1016/s0196-8904(98)00025-9.

[26] İbrahim Dinçer and Rosen, M.A. (2010). Thermal Energy Storage. doi:https://doi.org/10.1002/9780470970751.

[27] Khudhair, A.M. and Farid, M.M. (2004). A review on energy conservation in building applications with thermal storage by latent heat using phase change materials. Energy Conversion and Management, 45(2), pp.263–275. doi:https://doi.org/10.1016/s0196-8904(03)00131-6.

[28] Babich, M.W., Hwang, S.W. and Mounts, R.D. (1992). The search for novel energy storage materials using differential scanning calorimetry. Thermochimica Acta, 210, pp.83–88. doi:https://doi.org/10.1016/0040-6031(92)80279-6.

[29] Abbas, N., Awan, M.B., Amer, M., Ammar, S.M., Sajjad, U., Ali, H.M., Zahra, N., Hussain, M., Badshah, M.A. and Jafry, A.T. (2019). Applications of nanofluids in photovoltaic thermal systems: A review of recent advances. Physica A: Statistical Mechanics and its Applications, 536, p.122513. doi:https://doi.org/10.1016/j.physa.2019.122513.

[30] Koschenz, M. and Lehmann, B. (2004). Development of a thermally activated ceiling panel with PCM for application in lightweight and retrofitted buildings. Energy and Buildings, 36(6), pp.567–578. doi:https://doi.org/10.1016/j.enbuild.2004.01.029.

[31] Pielichowska, K. and Pielichowski, K. (2014). Phase change materials for thermal energy storage. Progress in Materials Science, 65, pp.67–123. doi:https://doi.org/10.1016/j.pmatsci.2014.03.005.

[32] Abdul Hussain Ayash, A. (2019). A NEW CORRELATION FOR SPECIFIC HEAT OF NORMAL ALKANES (C1-C30) AS A FUNCTION OF TEMPER-

ATURE AND CARBON NUMBER. Journal of Engineering and Sustainable Development, 23(3), pp.166–174. doi:https://doi.org/10.31272/jeasd.23.3.13.

[33] Sarı, A. and Kaygusuz, K. (2003). Some fatty acids used for latent heat storage: thermal stability and corrosion of metals with respect to thermal cycling. Renewable Energy, 28(6), pp.939–948. doi:https://doi.org/10.1016/s0960-1481(02)00110-6. b

[34] Sari, A. and Kaygusuz, K. (2002). Thermal performance of palmitic acid as a phase change energy storage material. Energy Conversion and Management, 43(6), pp.863–876. doi:https://doi.org/10.1016/s0196-8904(01)00071-1.

[35] Cabeza, L.F., Svensson, G., Hiebler, S. and Mehling, H. (2003). Thermal performance of sodium acetate trihydrate thickened with different materials as phase change energy storage material. Applied Thermal Engineering, 23(13), pp.1697–1704. doi:https://doi.org/10.1016/s1359-4311(03)00107-8.

[36] Liu, M., Saman, W. and Bruno, F. (2012). Review on storage materials and thermal performance enhancement techniques for high temperature phase change thermal storage systems. Renewable and Sustainable Energy Reviews, 16(4), pp.2118–2132. doi:https://doi.org/10.1016/j.rser.2012.01.020.

[37] Scopus, 2025. Scopus preview - Scopus - Welcome to Scopus. [online] Available at: https://www.scopus.com/record/display.uri?eid=2-s2.0-0019045167origin=inwardtxGid=0e87511dd5b641a8bc991b5993658202 [Accessed 17 Mar. 2025].

[38] Singh, P., Sharma, R.K., Ansu, A.K., Goyal, R., Sarı, A. and Tyagi, V.V. (2021). A comprehensive review on development of eutectic organic phase change materials and their composites for low and medium range thermal energy storage applications. Solar Energy Materials and Solar Cells, 223, p.110955. doi:https://doi.org/10.1016/j.solmat.2020.110955 (Singh et al., 2021).

[39] Wang, Z., Zhang, H. and Xia, X. (2017). Experimental investigation on the thermal behavior of cylindrical battery with composite paraffin and fin structure. International Journal of Heat and Mass Transfer, 109, pp.958–970. doi:https://doi.org/10.1016/j.ijheatmasstransfer.2017.02.057.

[40] Weng, J., He, Y., Ouyang, D., Yang, X., Zhang, G. and Wang, J. (2019). Thermal performance of PCM and branch-structured fins for cylindrical power battery in a high-temperature environment. Energy Conversion and Management, [online] 200, p.112106. doi:https://doi.org/10.1016/j.enconman.2019.112106.

[41] Sharma, D.K., Agarwal, P. and Prabhakar, A. (2023). Effect of fin design and continuous cycling on thermal performance of PCM-HP hybrid BTMS for high ambient temperature applications. Journal of Energy Storage, 74, pp.109360–109360. doi:https://doi.org/10.1016/j.est.2023.109360.

[42] Liu, Z., Wang, B., Tan, Y. and Li, P. (2023). Thermal management of lithium-ion battery pack under demanding conditions and long operating cycles using fin-enhanced PCMs/water hybrid cooling system. Applied thermal engineering, 233, pp.121214–121214. doi:https://doi.org/10.1016/j.applthermaleng.2023.121214.

[43] Influence of operational and design parameters on the performance of a PCM based heat exchanger for thermal energy storage – A

review. (2018). Journal of Energy Storage, [online] 20, pp.497–519. doi:https://doi.org/10.1016/j.est.2018.10.024.

[44] Suresh Kumar, K.R. and Kalaiselvam, S. (2017). Experimental investigations on the thermophysical properties of CuO-palmitic acid phase change material for heating applications. Journal of Thermal Analysis and Calorimetry, 129(3), pp.1647–1657. doi:https://doi.org/10.1007/s10973-017-6301-9.

[45] P. Manoj Kumar, M.S. Karuna, M.S. Sureshkumar, Moti Lal Rinawa, R. Sakthivel, K. Muthukumar and E. Kathir Malavan (2023). Evaluating the effect of magnesium oxide nanoparticles on the thermal energy storage characteristics of the inorganic PCM. Materials Today: Proceedings. doi:https://doi.org/10.1016/j.matpr.2023.02.297.

[46] B Kalidasan, Pandey, A.K., R. Saidur, Belqasem Aljafari, Yadav, A. and M Samykano (2023). Green synthesized 3D coconut shell biochar/polyethylene glycol composite as thermal energy storage material. Sustainable Energy Technologies and Assessments, 60, pp.103505–103505. doi:https://doi.org/10.1016/j.seta.2023.103505.

[47] Lin, S.C. and Al-Kayiem, H.H. (2016). Evaluation of copper nanoparticles – Paraffin wax compositions for solar thermal energy storage. Solar Energy, 132, pp.267–278. doi:https://doi.org/10.1016/j.solener.2016.03.004.

[48] Narayanan, S.S., Kardam, A., Kumar, V., Bhardwaj, N., Madhwal, D., Shukla, P., Kumar, A., Verma, A. and Jain, V.K. (2017). Development of sunlight-driven eutectic phase change material nanocomposite for applications in solar water heating. Resource-Efficient Technologies, 3(3), pp.272–279. doi:https://doi.org/10.1016/j.reffit.2016.12.004.

[49] Buonomo, B., Manca, O., Nardini, S. and Plomitallo, R.E. (2022). Numerical study on latent heat thermal energy storage system with PCM partially filled with aluminum foam in local thermal equilibrium. Renewable Energy, 195, pp.1368–1380. doi:https://doi.org/10.1016/j.renene.2022.06.122.

[50] Zhu, Z., Huang, Y., Hu, N., Zeng, Y. and Fan, L. (2018). Transient performance of a PCM-based heat sink with a partially filled metal foam: Effects of the filling height ratio. Applied Thermal Engineering, 128, pp.966–972. doi:https://doi.org/10.1016/j.applthermaleng.2017.09.047.

[51] Joshi, V. and Rathod, M.K. (2019). Thermal performance augmentation of metal foam infused phase change material using a partial filling strategy: An evaluation for fill height ratio and porosity. Applied Energy, 253, p.113621. doi:https://doi.org/10.1016/j.apenergy.2019.113621.

[52] Marri, G.K. and Balaji, C. (2021). Experimental and numerical investigations on the effect of porosity and PPI gradients of metal foams on the thermal performance of a composite phase change material heat sink. International Journal of Heat and Mass Transfer, 164, p.120454. doi:https://doi.org/10.1016/j.ijheatmasstransfer.2020.120454.

[53] Iasiello, M., Mameli, M., Sauro Filippeschi and Bianco, N. (2021). Metal foam/PCM melting evolution analysis: Orientation and morphology effects. Applied Thermal Engineering, 187, pp.116572–116572. doi:https://doi.org/10.1016/j.applthermaleng.2021.116572.

[54] Diani, A. and Rossetto, L. (2021). Melting of PCMs Embedded in Copper Foams: An Experimental Study. Materials, [online] 14(5), p.1195. doi:https://doi.org/10.3390/ma14051195.

[55] Li, W.Q., Qu, Z.G., He, Y.L. and Tao, W.Q. (2012). Experimental and numerical studies on melting phase change heat transfer in open-cell metallic foams filled with paraffin. Applied Thermal Engineering, 37, pp.1–9. doi:https://doi.org/10.1016/j.applthermaleng.2011.11.001.

[56] Mancin, S., Diani, A., Doretti, L., Hooman, K. and Rossetto, L. (2015). Experimental analysis of phase change phenomenon of paraffin waxes embedded in copper foams. International Journal of Thermal Sciences, 90, pp.79–89. doi:https://doi.org/10.1016/j.ijthermalsci.2014.11.023.

[57] Rehman, T. and Park, C.W. (2024). Optimising heat sink performance with porous media–PCM integration: An experimental investigation. Applied Thermal Engineering, 242, pp.122506–122506. doi:https://doi.org/10.1016/j.applthermaleng.2024.122506.

[58] Ieee.org. (2024). Benefits and Challenges of PCM-Based Thermal Management at the Die and Component Level. [online] Available at: https://ieeexplore.ieee.org/abstract/document/10534920 [Accessed 5 May 2025].

[59] Bian, Z., Hou, F., Chen, J. and Wang, H. (2024). Numerical analysis on the effect of graded porosity in closed-cell metal foams/PCM composites. Case Studies in Thermal Engineering, [online] 55, p.104145. doi:https://doi.org/10.1016/j.csite.2024.104145.

[60] Kotb, A. and Wang, S. (2024). Enhanced thermal storage performance with non-linear porosity distribution in copper foam-PCM composites. Journal of Energy Storage, [online] 105, p.114612. doi:https://doi.org/10.1016/j.est.2024.114612.

[61] Maxa, J., Novikov, A. and Nowottnick, M. (2017). Thermal Peak Management Using Organic Phase Change Materials for Latent Heat Storage in Electronic Applications. Materials, 11(1), p.31. doi:https://doi.org/10.3390/ma11010031.

A

Appendix 1

Lorem ipsum dolor sit amet, consectetur adipisicing elit, sed do eiusmod tempor incididunt ut labore et dolore magna aliqua. Ut enim ad minim veniam, quis nostrud exercitation ullamco laboris nisi ut aliquip ex ea commodo consequat. Duis aute irure dolor in reprehenderit in voluptate velit esse cillum dolore eu fugiat nulla pariatur. Excepteur sint occaecat cupidatat non proident, sunt in culpa qui officia deserunt mollit anim id est laborum.

DEPARTMENT OF SOME SUBJECT OR TECHNOLOGY
CHALMERS UNIVERSITY OF TECHNOLOGY
Gothenburg, Sweden
www.chalmers.se

CHALMERS
UNIVERSITY OF TECHNOLOGY